ITER Physics Basis
Chapter 1, Overview and Summary

ITER Physics Basis Editors[*], ITER Physics Expert Group Chairs and CoChairs[**],
and ITER Joint Central Team and Physics Integration Unit[***]

* ITER Physics Basis Editors: F. W. Perkins, D. E. Post, N. A. Uckan, M. Azumi, D. J. Campbell, N. Ivanov, N. R. Sauthoff, M. Wakatani
Additional contributing editors: W. M. Nevins, M. Shimada, J. Van Dam

** ITER Physics Expert Group Chairs and Co-Chairs: D. Boucher, G. Cordey, A. Costley, J. Jacquinot, G. Janeschitz, S. Mirnov, V. Mukhovatov, G. Porter, D. Post, S. Putvinski, M. Shimada, R. Stambaugh, M. Wakatani, J. Wesley, K. Young

** ITER Joint Central Team and Physics Integration Unit: R. Aymar, Y. Shimomura, D. Boucher, A. Costley, N. Fujisawa, Y. Igitkhanov, G. Janeschitz, A. Kukushkin, V. Mukhovatov, F. Perkins, D. Post, S. Putvinski, M. Rosenbluth, J. Wesley

Abstract

The ITER Physics Basis presents and evaluates the physics rules and methodologies for plasma performance projections which provide the basis for the design of a tokamak burning plasma device whose goal is to demonstrate the scientific and technological feasibility of fusion energy for peaceful purposes. This Chapter summarizes the physics basis for burning plasma projections which is developed in detail by the ITER Physics Expert Groups in subsequent chapters. To set context, the design guidelines and requirements established in the report of ITER Special Working Group 1 are presented, as are the specifics of the tokamak design developed in the Final Design Report of the ITER Engineering Development Activities, which exemplifies burning tokamak plasma experiments. The behaviour of a tokamak plasma is determined by the interaction of many diverse physics processes, all of which bear on projections for both a burning plasma experiment and an eventual tokamak reactor. Key processes summarized here are: energy and particle confinement and the H-mode power threshold; MHD stability, including pressure and density limits, neoclassical islands, error fields, disruptions, sawteeth, and ELMs; power and particle exhaust, involving divertor power dispersal, helium exhaust, fuelling and density control, H-mode edge transition region, erosion of plasma facing components, tritium retention; energetic particle physics; auxiliary power physics; and the physics of plasma diagnostics. Summaries of projection methodologies, together with estimates of their attendant uncertainties, are presented in each of these areas. Since each physics element has its own scaling properties, an integrated experimental demonstration of the balance between the combined processes which obtains in a reactor plasma is inaccessible to contemporary experimental facilities: it requires a reactor-scale device. It is argued, moreover, that a burning plasma experiment can be sufficiently flexible to permit operation in a steady-state mode, with non-inductive plasma current drive, as well as in a pulsed mode where current is inductively driven. Overall, the ITER Physics Basis can support a range of candidate designs for a tokamak burning plasma facility. For each design, there will remain a significant uncertainty in the projected performance, but the projection methodologies outlined here do suffice to specify the major parameters of such a facility and form the basis for assuring that its phased operation will return sufficient information to design a prototype commercial fusion power reactor, thus fulfilling the goal of the ITER project.

IPB-CHAPTER 1

OVERVIEW: INTRODUCTION AND SUMMARY

TABLE OF CONTENTS

1. OVERVIEW: INTRODUCTION AND SUMMARY

1.1. INTRODUCTION

Magnetic fusion energy research has reached the point where a tokamak burning plasma facility in which the thermonuclear heating balances (or is comparable to) transport and radiation losses for periods of 1000 s or longer can be seriously contemplated as an appropriate next step. Achieving this goal would be a major step forward, both in science and in technology, towards the ultimate goal of magnetic fusion generation of electrical power with significant environmental advantages [1, 2] Overall, such a facility would have a size, magnetic field strength, physics phenomenology, and technological basis very close to that of an eventual thermonuclear power reactor, be it a tokamak or some other toroidal configuration. Indeed, three aspects of the interplay between physics and technology are common to a burning plasma experiment and a reactor. First, the general confinement properties of a tokamak device which achieves such a thermal balance implies a power level of ~1GW and a neutron wall loading of ~1 MW/m^2 — levels in the range anticipated for commercial power production. Second, in the proposed tokamak configuration, be it a reactor or burning plasma experiment, the magnitude of the magnetic field needed to confine stably a plasma of sufficient pressure to generate ~1GW of fusion power is comparable to the limiting magnetic fields which a toroidal superconducting magnet can produce. Third, the linear size of the plasmas is sufficiently larger than the shield thickness needed to protect superconducting magnets from nuclear radiation, so that the shield occupies only a modest fraction of the volume available inside the confining magnets and does not dominate the design. Appendix A adds details to these arguments. As a consequence, data from such a burning plasma facility is foreseen to require little extrapolation to an experimental power reactor and is essential to defining its principal operational mode. For example, if a steady-state operational mode is to be chosen for a commercial tokamak reactor design, then this choice must rest on a robust experimental demonstration of steady-state physics and operation in a burning plasma experiment.

It is therefore noteworthy that, in the worldwide fusion research program, tokamak experiments have demonstrated a common plasma physics across a range of device sizes, magnetic field strengths, and auxiliary heating powers. This common physics provides the basis for moving ahead with a burning plasma facility by permitting development of extrapolation principles, both theoretical and empirical, and their application to the projection of burning plasma performance. It is the role of this Article to summarize and assess the qualitative and quantitative aspects of tokamak physics and to develop recommended extrapolation methodologies together with uncertainty estimates and physics design specifications for use by the designers of the burning plasma facility, which is called ITER — the International Thermonuclear Experimental Reactor.

Assessments of projections for plasma physics performance carried out by the seven ITER Physics Expert Groups in coordination with the ITER Physics Basis Editors and the Joint Central Team (JCT) form the core of this Article — Chapters 2-6. Chapter 7 assesses plasma measurement requirements and the extrapolation of physics principles on which diagnostic techniques are based. The final two chapters look forward to issues impacting the operation of a burning plasma facility and its experimental physics program.

The *ITER Physics Basis* has been compiled and written by a collaboration of authors that is based upon the seven ITER Physics Expert Groups, the *ITER Physics Basis* Editors, and physics staff from the ITER Joint Central Team (JCT), supplemented in the various Chapters by physics and technology specialists drawn from the plasma research programs of the ITER Parties. The Expert Group Chairs and Co-chairs and the *ITER Physics Basis* Editors played a key role in the final compilation and editing. Within their own areas of expertise, each of the Expert Groups has been evaluating progress and recommending priorities for physics research in the Four Parties physics research programs. Consequently, their members have acquired the physics expertise and burning plasma perspective needed to develop and assess projection methodologies.

The ITER/EDA procedure has been to base design choices on the physics principles discussed and documented in this Article. ITER design issues and decisions, which are the

responsibility of the Joint Central Team, are documented in the physics chapter of the ITER Final Design Report [3, 4] and in the Physics Design Description Documents [5]

This Introduction is written as a summary of the entire Article and as such provides an overview and integration of the separate Chapters. To establish context, Section 1.2 will describe the ITER Agreement and the current Engineering Design Activities (ITER/EDA) as well as the specifications that the device under design must fulfill. The design parameters documented in the ITER Final Design Report (FDR) are presented as exemplifying reactor-scale devices. It should be stressed that the projection methodolgies reported in this Article apply to a range of parameters and form a basis for assessing tradeoffs associated with reduced-cost designs relative to the FDR design.

Section 1.3 summarizes the main content of this Article — the identification of the various physics processes in contemporary tokamaks and their projection principles. Next, Section 1.4 argues that the dominant physics in a reactor-scale facility will differ in important ways from that in present devices. An example is the integration of core transport and edge physics. Our discussion organizes the differences into three elements and outlines the scientific knowledge that operation of a reactor-scale facility will return. This Introduction concludes with an assessment of the physics projection methodologies supporting design of a reactor-scale experiment.

1.2. ITER

The importance of the step to reactor-scale devices motivated the governments of the Four Parties — the European Union, Japan, the Russian Federation, and the United States — to initiate in 1987 the International Thermonuclear Experimental Reactor/Conceptual Design Activities (ITER/CDA). The promise of the Conceptual Design, which was completed in 1990 [6] led in 1992 to the present ITER Engineering Design Activities (ITER/EDA) Agreement [7] aimed at developing a detailed engineering design for a reactor-scale tokamak facility that would achieve controlled ignition and extended burn. As envisioned by the Agreement, the ITER device would be the central element of an international, one-step-to-a-reactor strategy.

1.2.1. ITER: Backgound and Mandate

The overall goal of ITER/EDA, as set forth in Article 1 of the ITER Agreement (Appendix B), is to demonstrate the scientific and technological feasibility of fusion energy for peaceful puposes. Special Working Group 1 was chartered by the ITER Council to develop detailed technical objectives for the ITER design to assure that the design would fulfill this overall goal. The report of SWG1 can be found in Appendix C. This report makes it clear that the device which results from the EDA should not only achieve controlled ignition and extended burn in established favorable confinement modes, but also should be sufficiently flexible to provide access for the introduction of advanced features and new capabilities and to allow for optimizing plasma performance during operation. Steady-state experiments should aim at a demonstration of steady-state operation in plasmas having alpha particle heating power at least comparable to externally applied power. The choice of parameters should be consistent with margins that give confidence in achieving the required plasma performance.

In brief, the ITER device is to be a flexible, reactor-scale experimental facility capable of standard and advanced operating modes. It is envisioned to be the world's first reactor-scale magnetic fusion experiment and as such will be the first to combine the elements discussed above: a capability for achieving sustained ignition and extended-duration fusion burn in deuterium-tritium (DT) plasmas with reactor-relevant engineering features that include superconducting magnet systems, remotely-maintainable in-vessel nuclear shielding, and plasma-facing components with steady-state power and particle exhaust capabilities.

1.2.2. ITER: FDR Design

The approximate magnitude of the parameters for an ignited, reactor-scale tokamak can be derived from simple arguments, which are set forth in Appendix A and based on operation in the the favorable ELMy H-mode confinement regime. In this regime, plasma turbulent heat

conduction spontaneously diminishes in a thin, transport-barrier layer just inside the magnetic separatrix. This layer is commonly observed to undergo succesive relaxations called Edge Localized Modes — ELMs. The interest in ELMy H-modes flows from experimental observations that show this mode reduces transport throughout the plasma core. The standard working hypothesis, supported by many observations, is that H-mode occurs when the power transported across the separatrix exceeds a threshold value.

Table 1.1 and Fig. 1-1 present the specifics of the ITER Design which follow from the arguments of Appendix A and supporting detailed design calculations [4] . Since the arguments are straight-forward, ITER truly exemplifies a tokamak reactor facility. Quantitative calculations based on parameters close to those of Table 1.1 will be representative of any reactor-scale tokamak facility with an ignition capability. These parameters fullfill a self-consistency check that the power transported through the separatrix exceeds the threshold power required to maintain H-mode confinement. Table 1.1 takes into account the favorable isotope effect on threshold power confirmed in recent JET DT experiments [8] One notes that the optimized ignition condition depends sensitively on plasma size and magnetic field strength (Eq.A-4 of Appendix A), so that fusion performance degrades for device sizes less than that of the FDR design. Increased magnetic field strength can restore performance loss resulting from decreased plasma size.

While ITER is designed to ignite, i.e. to produce enough fusion power to overcome heat losses, auxiliary power is required to initially raise the plasma temperature as well as for control and current drive purposes. Auxiliary heating power in the range 50-150 MW can take the form of negative-ion based 1 MeV neutral beam injection, ion-cyclotron heating by the fast magnetosonic Alfven wave, and electron cyclotron heating. These auxiliary heating systems also possess a current drive capability and electron cyclotron heating is notable in that its current drive can be utilized for current profile control. Lower hybrid current drive is also under study for later investigations of steady-state operation. Neutral beam injection is unique in its capability to introduce angular momentum.

Figure 1.1 presents a poloidal plane view of the ITER facility and Figure 1.2 gives representative density and temperature profiles for an ignited ITER discharge. Because there is essentially no ionization occuring inside the separatrix, the density profile is flat. Any density gradient close to the separatrix would be sensitive to details of fuelling and not essential to performance calculations, which rest on core thermonuclear and auxiliary heating as well as core transport.

Table 1.1. ITER Design Features and Parameters for Reference Ignited ELMy H-mode Operation

Parameter	Value
Major/minor radius	8.14 m/2.80 m
Plasma configuration	Single null divertor
Plasma Vertical elongation/triangularity (at 95% poloidal flux)	1.6/0.24
Plasma volume	~2000 m^3
Plasma surface area	~1200 m^2
Nominal plasma current	21 MA
Electron Density	$0.98 \cdot 10^{20}$ m^{-3}
Volume Average Temperature	12.9 keV
Toroidal field	5.68 T (at R = 8.14 m)
MHD safety factor (q_{95})	~3.0 (at 21 MA)
Volume average β / β_N	0.030 / 2.29
Fusion power (ignited, nominal)	1.5 GW
Plasma thermal energy content	1.07 GJ
Plasma magnetic energy content	1.1 GJ
Confinement Mode	ELMy H-mode
Radiation from plasma core	118 MW
Transport Power Loss	182 MW
Transport Energy Confinement time τ_E	5.9 sec
$P_{transport}/P_{L\rightarrow H}$	1.4
Species Concentrations % He/Be/Ar	10 / 2 / 0.16
Z_{eff} - effective ion charge	1.9
Average neutron wall loading	~1 MW/m^2 (at 1.5 GW)
Lifetime neutron fluence	$\geq$ 1 MWa/m^2
Burn duration (ignited, inductive current drive)	$\geq$ 1000 s
Available auxiliary heating power	100-150 MW
In-vessel tritium inventory safety limit	1 kg

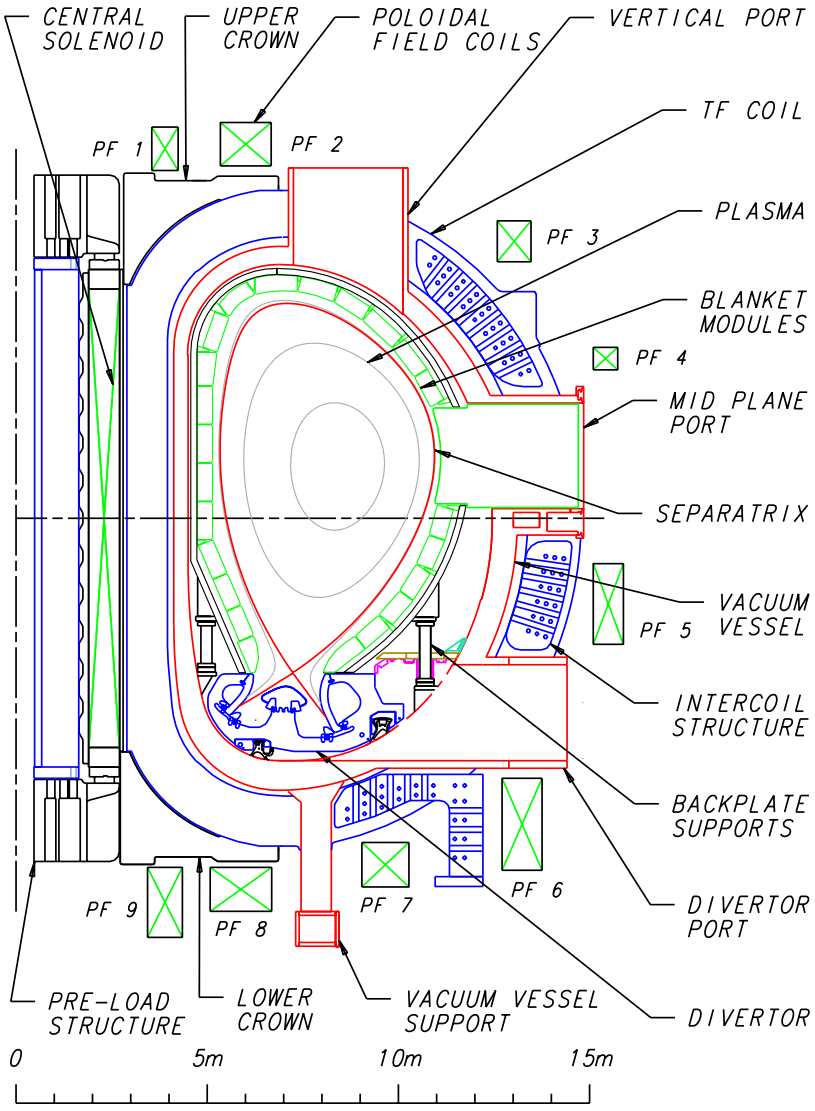

FIG. 1-1. Poloidal Plane View of the ITER FDR design. Closed curves in the plasma region depict magnetic surfaces the confining magnetic field lies on these surfaces. The separatrix magnetic surface (single red contour) defines the boundary between magnetic surfaces which close within the plasma region and those which intersect material walls.

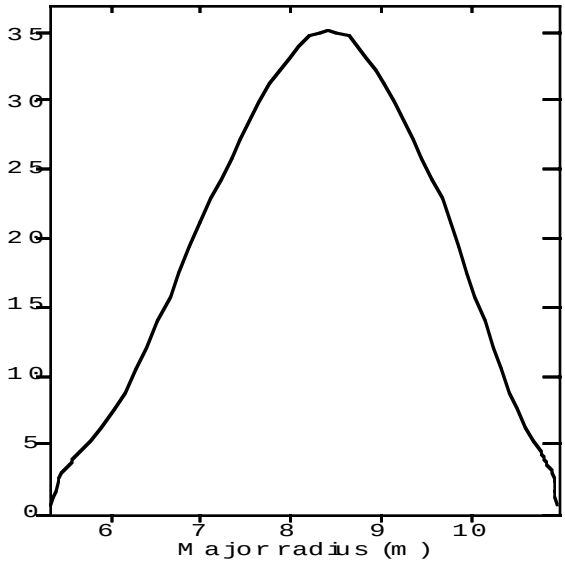

Figure 1-2a: Ion Temperature profile (keV) corresponding to the plasma of Table 1.1. Electron and ion temperatures are close to equal.

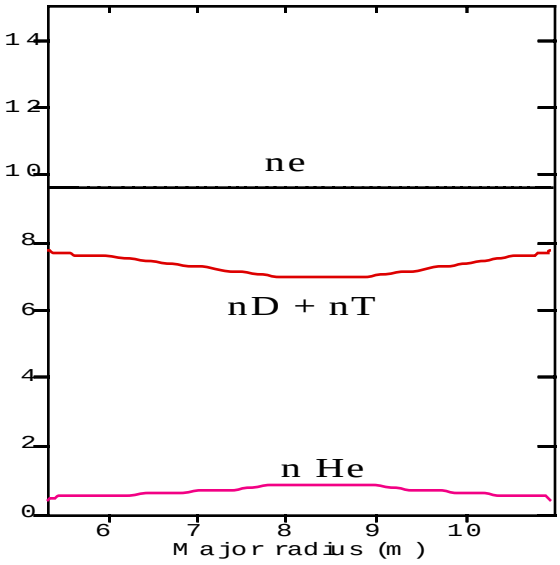

Figure 1-2b: Electron, DT ion and He density profiles (10^{19} m^{-3}) for the plasma of Table 1.1.

How big a step is the ITER FDR device? Figure 1.3 compares the fusion figure-of-merit $M = n_{DT}(0)\cdot T_i(0)\cdot\tau_E$ for present tokamaks with the values computed for ITER under minimum ignition conditions, which require $M \approx 110$. Here τ_E denotes the thermal energy confinement time in sec, $n_{DT}(0)$ the central DT fuel density in units of $10^{20}m^{-3}$, and $T_i(0)$ the central ion temperature in keV. ITER FDR parameters lie a factor-of-1.5 in magnetic field strength and a factor-of-2.9 in linear size beyond the latest JET DT ELMy H-mode discharges [9]. The increase in the figure-of-merit from ITER-like discharges in present devices to ITER is appreciable (a factor of 40), but comparable to the range of M spanned by ITER-like ELMy H-mode discharges in present experiments (also a factor of 40). It is likewise in accord with the expected increase resulting from increases in magnetic field strength and size, according to Appendix A, Eq. (A-5).

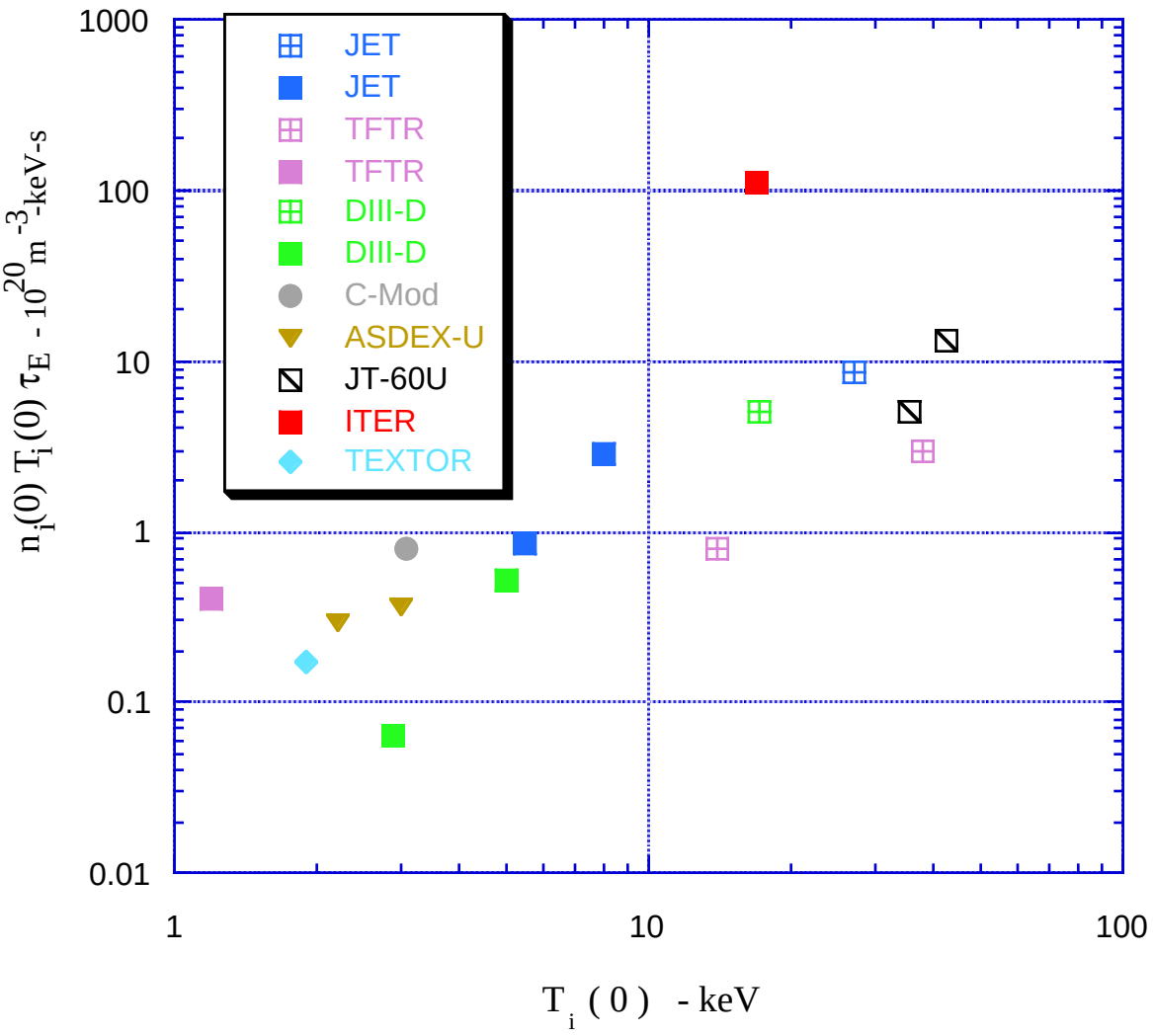

FIG. 1.3. Fusion figure of merit $M = n_i(0)\ T_i(0)\ \tau_E$ for selected tokamak discharges. Filled symbols represent steady discharges with $T_e \approx T_i$ in H-mode, except for TEXTOR, which is in a radiation-enhanced mode, and for TFTR in a pellet fueling mode. Open symbols represent confinement modes with $T_i >> T_e$ which have been optimized for fusion output. The ITER point represents the minimum M for steady, ignited burn and is insensitive to $T_i(0)$ because of β limits.

Tokamaks have already entered the regime of thermonuclear burning [8-12]. Figure 1.4 summarizes results from JET and TFTR. These experiments document that the expected heating from thermonuclear α-particles is occurring. We note that long-pulse ELMy H-mode results from JET are limited by the available auxiliary heating power which is insufficient, at a toroidal field strength of 3.8 T, to reach β_N values characteristic of a reactor. Figure 1.3 also contains points at higher values of M based on hot-ion and supershot modes especially optimized for present devices such as JET, JT-60U, and TFTR. These high-T_i confinement modes rely on $T_i >> T_e$, which, as a rule, is inaccessible to burning plasmas because: 1) α-particles principally heat electrons as a result of their high energy and 2) the electron-ion temperature equilibration time ($\tau_{eq} \approx$ 0.5s) is shorter than the energy confinement time ($\tau_E \approx$6s) in a reactor-scale device. In present experiments, the energy of injected particle beams is such that they principally heat ions. Moreover, since the equilibration time is comparable to the energy confinement time $\tau_E \approx \tau_{eq}$, the resulting plasma has $T_i >> T_e$.

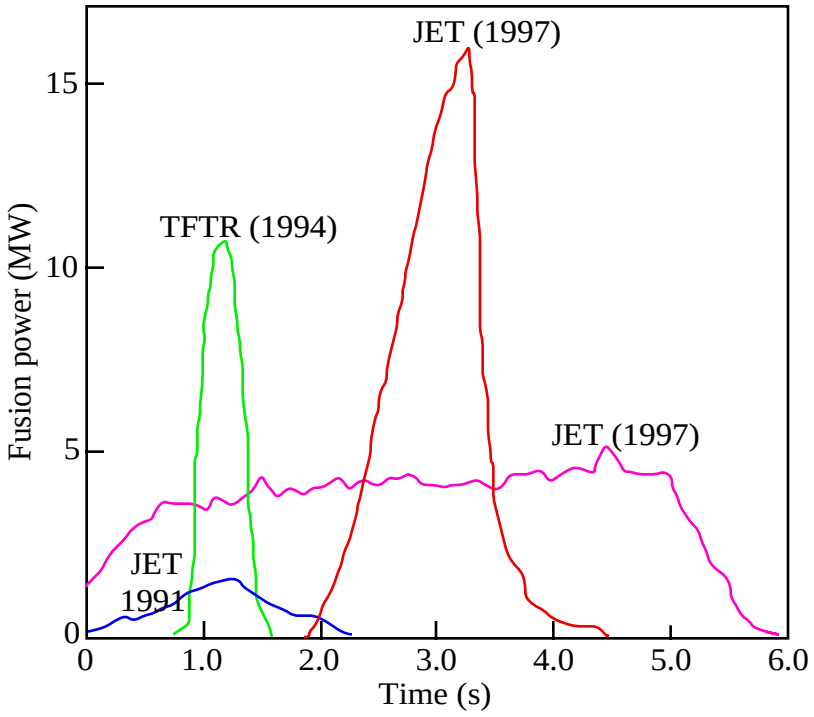

FIG. 1.4. Thermonuclear power generation in TFTR and JET versus time (arbitrary zero). The long duration JET power generation is for an ITER-like ELMy H-mode.

It follows that an ignited burning plasma objective (M>110) for the EDA design is a large step, but one which is commensurate with the available database.

1.3. TOKAMAK PHYSICS PROCESSES AND PROJECTION PRINCIPLES

Tokamak physics has reached a level that supports the detailed design of a new, large facility. To a very good approximation, a tokamak is a figure-of-revolution. The resulting property of axisymmetry reduces computation of the force balance between plasma pressure gradients and **j**x**B** forces to the solution of a single 2-dimensional partial differential equation called the Grad-Shafranov equation [13]. Sophisticated computational solutions yield accurate and experimentally-validated descriptions of a tokamak plasma internal structure and boundaries and also predict

precisely how they respond to externally applied shaping fields. Stability of these plasmas with respect to small, symmetry-breaking pertubations can also be accurately assessed by highly developed variational techniques provided the perturbations obey the ideal magnetohydrodynamic constraint, wherein very high plasma conductivity permits one to neglect the component of the plasma electric field which lies parallel to the magnetic field. Computation of plasma heating and fuelling is also straightforward and sophisticated codes exist that yield experimentally-validated, first principles profiles of energetic-particle creation, plasma heating, non-inductive current drive, and particle deposition.

Experiment has shown that, once an ideally-stable equilibrium is assured, the plasma response to auxiliary heating and fuelling is governed by transport introduced by the spontaneous appearence of both fine-scale and global symmetry-breaking fluctuations in which the small-but-finite parallel component of the plasma electric field plays an essential role. In the edge region, the additional complexities of plasma-atomic physics and plasma-surface interactions enter. Contemporary tokamak physics concerns itself with the consequences of these small but crucial deviations from the fundamental axisymmetric equilibrium.

The physics basis for projecting reactor-scale plasma performance must begin with identification of the fundamental plasma, atomic, and surface physics phenomena occuring in tokamak plasmas and their supporting qualitative theoretical descriptions. Quantification then rests on experimental data from the present generation of devices, which has benefited from databases developed during the EDA. From this, one must develop theoretical/computational (or at least well-documented empirical) methodologies for extrapolation to a reactor-scale device. The magnitude of the global fusion energy research effort attests to the fact that fusion plasmas are complex, with diverse plasma and plasma-surface interaction phenomena occuring simultaneously. Each process requires an extrapolation to ITER. In these circumstances, we can bring experimental and theoretical information to bear on identifying the qualitative features and scaling

properties of the fundamental physics phenomena. Quantitative predictions flow from the normalization of scaling relations to data from a range of tokamaks. In systems such as tokamaks where many individual process are at work, a second source of complexity associated with the interactions between fundamental processes also enters. Examples include 1) the plasma periphery where atomic radiation processes are a dominant phenomena in the plasma thermal balance and 2) simulations of integrated performance. In such cases, modeling codes replace analytic scaling relations as the preferred methodology for prediction of reactor plasma performance.

1.3.1. General Projection Issues

How is confidence to be established for projection of plasma properties to ITER-scale devices? There are two fundamental approaches. The first is theoretical, where the qualitative features, and sometimes quantitative aspects, of physics processes can be understood in terms of a theoretical model — often in the form of a sophisticated code. An example is energetic particle losses caused by imperfections in the confining magnetic fields. One can then validate the model by comparison with data from a range of tokamaks. Conversely, the lack of a predictive theoretical model, as is presently the case for the H-mode power threshold, is a cause for concern in that unknown limitations may apply. The second source of confidence is that projections rest on a common physics observed across a range of tokamak discharges spanning a factor of 6 in linear dimension, a factor of 6 in magnetic field strength, and a factor of 34 in plasma current. Uncertainties in projections can then be related to the degree of precision with which scaling formulas or predictive codes can quantatively represent the common physics. Physics that cannot be reproduced across this spectrum of discharges is not appropriate for use in design-basis projections for next-step machines, except when there is a compelling theoretical reason to the contrary.

The starting point for our characterization of ITER physics processes is Figure 1-5, which portrays a representative “single null” divertor plasma equilibrium. In this Figure, it is useful to identify four regions in which different dominant physics prevails, but where there can be

important interactions at the boundaries. The four regions are: 1) the core, 2) the edge pedestal region just inside the separatrix, 3) the scrape off layer (SOL) plasma just outside the separatrix, and 4) the divertor chamber plasma region,which is an extension of the SOL plasma along field lines into the divertor chamber. Within a given region, a subdivision into short-scale and global processes is also beneficial.

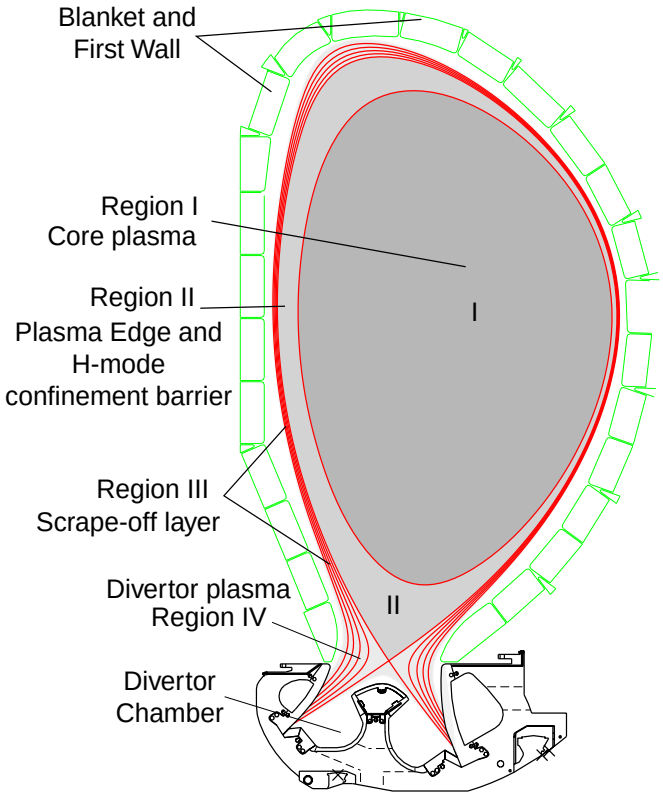

FIG. 1.5. Poloidal plane view of ITER, illustrating four principal regions where dominant physics differs. The separatrix, which forms the boundary between Regions II and III, possess a point of null poloidal field strength where it has the "X" crossing. Configrations of this type are referred to as "single-null" plasmas.

Further insight can be gained by recognizing that most of the physics processes are the result of quasi-neutral plasma physics where, to a high degree of approximation, $\nabla \cdot \mathbf{j} = 0$ and electron and ion charge densities can be taken as equal. Here $\mathbf{j}$ denotes the plasma current density. When quasi-neutrality holds, Kadomstev [14] pointed out that general scalings could be cast into nondimensional forms that involve only three dimensionless plasma quantities, in addition to

dimensionless geometric quantities such as the inverse rotational transform q, elongation κ, etc. The conventional choice for these three parameters has been

$$\rho^* = \frac{\text{ion gyroradius}}{\text{minor radius}} = \left(\frac{2T_i}{M_i}\right)^{1/2} \frac{M_i}{eBa} \qquad \beta = \frac{\text{plasma pressure}}{\text{magnetic pressure}} = \frac{2\,\mu_o\, n\left(T_e + T_i\right)}{B^2} \tag{1.3-1}$$

$$\nu^* = \frac{\text{connection length}}{\text{trapped particle mean–free–path}} = \nu_{ii}\left(\frac{M_i}{T_i}\right)^{1/2}\left(\frac{R}{r}\right)^{3/2} qR \tag{1.3-2}$$

$$\nu_{ii} = \left(\frac{4\sqrt{\pi}}{3}\right)\frac{n_i e^4 \ell n\Lambda}{M_i^{1/2} T_i^{3/2}} \tag{1.3-3}$$

In these formulas, the temperature is expressed in energy units (joules). For global parameters, one can use T =2W/3N, where W is the plasma energy content and N its particle inventory of electrons and ions.

Because of variations in magnetic field strength in a tokamak, some particles execute a bouncing-type trajectory caused by the magnetic mirroring property of particle orbits in non-uniform magnetic fields (see ref [13] p 42). Definition (1.3-2) emphasizes bouncing particles as the key physics which binary collisions alter. Other definitions of collisionality involving, for example, temperature equilibration, could be used instead. Whenever possible, we cast our extrapolations in dimensionless form to assure adherence to Kadomstev's principle and we refer to these extrapolations as being "dimensionally correct". In the plasma periphery, and especially in the divertor plasma, neutral atom and atomic radiation processes become important and Kadomstev's principle no longer applies.

The importance of dimensionless parameters leads to the concept of ITER Demonstration Discharges, in which Region 1 physics is matched as closely as possible to a reactor in terms of dimensionless parameters, including profile and magnetic geometry parameters. It is found that discharges in present tokamak facilities can be formed with values of β and ν^* identical to reactor values but with ρ^* having a factor of 5 greater value. This reduces the problem of extrapolation

from three parameters to a single parameter, ρ^*, as discussed in Chapter 2.7. Under these constraints, the density and temperature scale according to

$$n \propto \left(\beta^2 \nu^*\right)^{1/3} B^{4/3} R^{-1/3} \qquad T \propto \left(\beta / \nu^*\right)^{1/3} B^{2/3} R^{1/3} \tag{1.3-4}$$

Figure 1.6 portrays a JET ELMy H-mode discharge with such features and Table 1.2 gives relevant parameters. Its confinement is very close to that predicted by the latest ELMy H-mode scaling relation to be found in Eq.(1.3.2-1) and Fig.2.6-1. The relative plasma pressure, as defined by $\beta_N = 100\ \beta\ (aB/I_{p,MA})$ using MKS units, has a value close to that planned for ITER, but the nondimensional collisionality ν^* is modestly larger that the nominal ITER discharge of Table 1.1.

Table 1.2. Parameters of a JET D-T ITER Demonstration Discharge

Parameter	Value
Shot Number	42756
B (T) toroidal field at axis	2.0
I (MA) plasma current	2.0
R (m) major radius	2.9
a (m) minor radius	0.93
q_{95} measure of magnetic twist	3.4
κ/δ elongation/ triangularity	1.76/0.2-0.3*
$\langle n \rangle$ / n_{GR} ($10^{19} m^{-3}$)	4.7 / 7.4
Z_{eff} effective ion charge	1.9
P (MW) Auxlliary heating power	17.3
P_{fusion} (MW) fusion power	2.1
W_{th} (MJ) plasma energy content	4.5
τ_{th} (sec) heat confinement time	0.26
$B\,\tau_{th}$	0.52
H_H	1.04
ν^*/ν^*_{ITER}	2.1
$\beta_{N,th}$ normalized pressure	2.25
$n(0)$ ($10^{20} m^{-3}$) plasma density	0.59
$n(0)_{ITER}$ †	1.6
$T_i(0)$, $T_e(0)$ (keV)	5.5, 5.0
$T_{i,ITER}$, $T_{e,ITER}$ (kev) †	16.0, 14.5
Divertor Status	Attached

*Range of values during pulse. † Scaled at constant β and ν^*

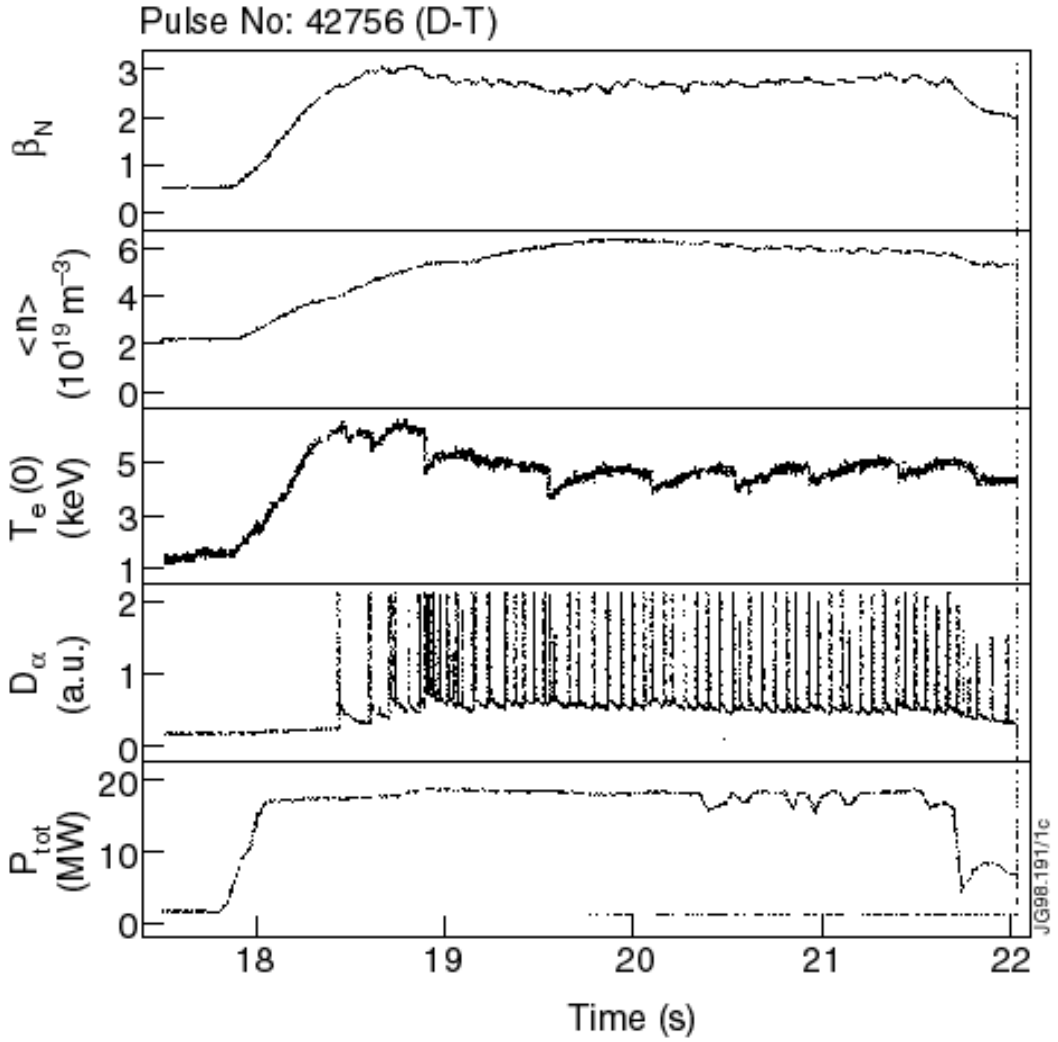

FIG. 1.6. JET D-T ELMy H-mode ITER Demonstration Discharge. Normalised β, line average electron density (10^{19} m^{-3}), central electron temperature $T_e(0)$ in keV, D_α and total power (MW) versus time for JET pulse 42756. See Table 1.2 for parameters. Divertor regime was attached.

The sudden relaxations of $T_e(0)$ are a generic tokamak phenomenon called "sawteeth", which are explained in Section 3.3.5 of this chapter. Sawteeth attest to the fact that the central q value is less than unity. This discharge is an integrated demonstration of the compatibility of un-degraded core confinement with core β_N limits, including pressure-driven modes centered on the

q=1 surface [15]. On the other hand, the "attached" divertor edge physics regime for this discharge differs from that of a reactor, as discussed in Section 1.4.

Further evidence for the nondimensional approach lies in the comparison of discharges prepared to have identical nondimensional parameters, but differing magnetic field, density, auxiliary power, etc. For these discharges, the Kadomstev principle predicts that a nondimensional energy confinement time defined by $\Omega_i\tau_E$ should be identical. Here Ω_i denotes the ion gyrofrequency and τ_E is the thermal energy confinement time $\tau_E = W/P$ where P is the thermal heating power. Chapter 2.7.2 reports a comparison between a DIII-D discharge and a nondimensionally identical JET discharge. The dimensionless energy confinement times are identical within 5% , which establishes the validity of the Kadomstev scaling principle over the size range between DIII-D and JET.

Next we turn to the central purpose of this Section: identification of the various plasma phenomena occurring in tokamaks and of the projection principles which apply to them.

1.3.2. Core Confinement and Transport

Chapter 2 addresses the anomalous core thermal transport arising in Region 1 from fine-scale plasma turbulence, whose characteristic scale size is small compared to the device size. The working hypothesis is that core transport is governed by core dimensionless physics variables through the core density, temperature, and magnetic field values. It is recognized that the properties of the Region 2 edge plasma could also affect core energy content, particularly if the core logarithmic temperature gradient is constrained to lie near marginal stability values.

1.3.2.1. Global confinement scaling

Confinement properties of tokamak plasmas have long been characterized by their global confinement time — the ratio of thermal energy content to heating power (in steady conditions). Two approaches are used to project values measured on present tokamaks to reactor-scale devices:

regression analysis of a confinement time database and the ρ^*-scaling of ITER Demonstration Discharges. Global regression projections for ITER rest on a database of ELMy H-mode discharges which has been considerably expanded and improved during the EDA. Log-linear (power law) regression analyses applied to this database generate confinement time scaling relations. Kadomstev nondimensional considerations impose a constraint equation among the power law exponents. A free-fit power law scaling relation satisfies this constraint to within statistical uncertainties. Consequently, this constraint is applied to the recommended power-law scaling relations to assure that they are dimensionally correct. As shown in Section 2.6, the scaling relation IPB98(y,1) based on the most complete set of ELMy H-mode data from 11 different tokamaks including all heating methods takes the form

$$\tau_E^{ELMy} = 0.0503 H_H \, I^{0.91} B^{0.15} P^{-0.65} n^{0.44} M^{0.13} R^{2.05} \varepsilon^{0.57} \kappa^{0.72} \qquad (3.2\text{-}1)$$

where the units are s, MA, T, MW, 10^{19} m^{-3}, amu, and m. H_H denotes a constant normally taken to be unity, and the elongation κ is defined as $\kappa = S_o/(\pi a^2)$ with S_o being the plasma poloidal cross-section area. Variations in H_H about unity are used in modeling studies [3] to ascertain the sensitivity of fusion performance to changes in confinement. During the EDA, much attention has been focussed on the uncertainty intervals associated with the recommended scaling relation. Section 6.4 of Chapter 2 addresses these issues.

The ELMy H-mode regression analyses are supplemented by ITER Demonstration Discharges prepared to have core nondimensional parameters as close to a reactor as possible. These discharges have β and ν^* values similar to a reactor but differ in ρ^*. H-mode scaling experiments which vary ρ^* at fixed β and ν^* find that confinement invariably lies close to the regression analysis prediction (3.2-1) whose ρ^*-scaling is almost that of the "natural" gyroBohm scaling theoretically predicted by simple dimensional analsis of equations for microinstability transport. The dimensional analysis argument rests on the fact that the scale of the turbulent fluctuations will exhibit a separation of spatial scale from the overall device and vary according to the ion gyroradius. Almost all first-principles microinstability simulations have gyroBohm scaling.

In addition to heat transport, transport of helium ash and angular momentum are important for reactor operations. The source of angular momentum is tangential neutral beam injection, which, together with the momentum diffusivity, determines the differential toroidal rotation rate. Section 10 of Chapter 2 reports that observations suggest momentum diffusivity is close to heat diffusivity. It is a subject of current research whether differential rotation can then close a loop and influence the diffusivity via differential rotation effects on microinstability growth rates and turbulence levels.

1.3.2.2. H-mode power threshold and pedestal

ITER confinement projections assume operation in the ELMy H-mode. Transport power losses from Region 1 must exceed the H-mode threshold power to assure that an edge transport barrier and pressure pedestal occur in Region 2. Such a power threshold requirement constitutes an important constraint on the operational space available to a fusion reactor [3, 4] Work during the EDA has created an extensive database of H-mode power thresholds [16-18] . Section 4 of Chapter 2 presents a resulting family of empirical scalings Eq.(2.4-2) for the L→H power threshold which are dimensionally correct, but which contain appreciable uncertainty caused by the necessity to determine a functional form for extrapolation from experimental data.

A considerable reduction in the power threshold uncertainty would result if a viable theoretical mechanism and theory-based scaling relation were available for extrapolation. Although half of the H-mode puzzle has been solved (we know that the transport reduction in the barrier arises from electric field shear [19]) these considerations have yet to produce a predictive theory for the scaling of the power threshold that triggers the evolution from L-mode to H-mode. Recent theoretical and computational simulation work [20-22] has introduced finite-β physics into threshold physics and the transport physics of Regions II and III in general. Dimensional analysis arguments indicate this step is essential for theory to recover the empirical threshold scalings. The simulation models do exhibit qualitative features of the Region II/III plasma, but do not yet have a full separatrix magnetic geometry needed for an accurate prediction of the power threshold.

Pedestal values of density and temperature just inside the H-mode transport barrier of Region II serve as boundary conditions for the Region I anomalous transport process. Transport and turbulence within Region 2, which determine the pedestal density and temperature values, is regarded as part of edge physics and treated in Section 3.7 of Chapter 4., mostly from perspective of a database to determine pedestal values. Pedestal temperatures can be very important if Region I temperature gradients are constrained to lie near a marginally stable logarithmic temperature gradient. First principles simulations of fine-scale turbulence are currently investigating whether Region I temperatures will be so constrained or will be relatively independent of pedestal boundary conditions. Even if Region I temperatures are reasonably independent of pedestal temperatures, the Region II pedestal energy content is generally not negligible compared to Region I energy content and can have a scaling which differs from the core scaling. In particular, pedestal energy content may be the source of the "isotope" effect common in confinement scalings such as (3.2-1) [23]. Indeed, work during the EDA has led to a greater general appreciation of the limitations which different scalings of different physics in different regions inevitably place on direct experimental investigation of the compatibility of the desired core and edge physics processes in reactor-scale plasmas.

1.3.2.3. Transport modeling and simulation

Figure 1-1 depicts representative magnetic surfaces in a tokamak plasma. The very rapid transport of heat and particles along a magnetic surface relative to the slow transport across surfaces has lead to a model of plasma transport wherin magnetic surfaces are regarded as iso-density, iso-temperature surfaces so transport only need be computed across magnetic surfaces. For cross-surface transport, the full shape of the magnetic surface is used in defining the volume element. Codes constructed in this approximation are called 1.5 dimensional transport models. Section 8 of Chapter 2 describes two different ways to predict the local energy transport coefficients (thermal diffusivity) for ITER from within a 1.5 dimensional transport modeling code. The first way, used in the PRETOR [24] code for FDR projections [4,5], consists of adjusting the

thermal diffusivity in such a manner that the global energy confinement time computed by the code is constrained to be equal to that given by a global scaling relation. The spatial profile of diffusivity is chosen so that temperature profiles are close to those observed in ITER Demonstration Discharges. This combined use of local transport coefficients adjusted to global scaling relations and of a 1.5 dimensional predictive transport code which can compute sources, sinks and boundary conditions – including some aspects of divertor physics – self-consistently with the predicted profiles is the most direct and reliable way to extrapolate the performance of a reactor-scale tokamak from present day experiments.

A second and more fundamental choice for local heat transport coefficients consists in using a model for the diffusity that does not depend on a global scaling relation but uses instead expressions for diffusivity and other transport coefficients that are drawn from theory-based considerations such as quasilinear theory, numerical plasma turbulence simulations, or simply dimensionally correct formulas motivated by observations. These models, once implemented in transport codes, can be used to predict temperature profiles which are then compared to experimental measurements available in the ITER Profile Database created during the EDA [25]. Predictions for some models are quite sensitive to the pedestal boundary temperature, because they are "stiff", meaning that the heat flux increases rapidly once the logarithmic temperature gradient exceeds a critical value. At present, many models are either still evolving, with new terms being added, or present too large a dispersion when compared to experimental results to allow reliable projection of ITER performances. On the other hand, a theory based expression such as the Multi-Mode model [26] is shown to achieve reasonable success when compared against experimental data and may therefore present a credible alternative to global scaling for ITER predictions. Presently predictions for ITER using this model come close to that using a diffusivity normalized to the global scaling relation, thereby providing an additional level of confidence to the overall performance projections.

Still more fundamental is computational simulation of turbulent transport coefficients or, more generally, the nonlinear heat-flux temperature-gradient relation. Two approaches are used: a

straightforward gyrokinetic particle simulation method [27] and the gyrofluid approach [28] . The gyrokinetic approach is more fundamental and uses particle simulation computational techniques in the 5-dimensional phase of microinstability turbulence — 3 spatial dimensions and 2 velocity space dimensions, energy and magnetic moment. Gyrofluid computations rest on velocity-space closure schemes that mimic kinetic effects and reduce the dimensionality of the computational space to three spatial dimensions. Different computational domains are used as well [29]. At this writing, the various approaches differ by up to a factor-of-8 in the heat flux for a given gradient. Resolution of these differences is in the research stage.

A fundamental understanding is needed to assess the prospects of the Radiation-Improved (RI) confinement mode studied on TEXTOR [30]. These observations find that confinement equals or exceeds that predicted by scaling relation (3.2-1) without the requirement to establish an H-mode edge barrier. Two central physics questions are: 1) What critical concentration of impurities is needed to alter microinstability turbulence to produce the characteristic RI-mode peaked density profiles and lower overall thermal losses than ordinary L-mode turbulent transport, even while permitting densities in excess of the Greenwald value, discussed in Section 3.3.8 of this Chapter? And 2), are the high fractional radiated powers associated with RI-mode impurity concentrations essential to altering the turbulent transport ? If a specific impurity concentration is required, then, in a reactor-scale device, radiation from the outer portion of Region 1, called the mantle, may exceed the available power because of the lower heating-per-unit-volume associated with a fusion energy source compared with auxiliary power deposition levels in present experiments. Of course, a reactor-scale facility will provide a test bed for experimental investigation of possible confinement improvements from injection of high-Z material, but a common physics over a variety of tokamaks, remains to be established before the RI-mode can be used as a design-basis for a reactor-scale facility.

1.3.2.4. Confinement and magnetic configuration

Many recent experiments in tokamaks indicate that transport arising from fine-scale turbulence is strongly influenced by the global magnetic configuration. Reverse-shear configurations are an evident example [31,32]. Even for the ELMy H-mode, the empirical scaling relations indicate a high sensitivity to elongation. Yet more dramatic are the numerous observations of internal transport barriers, documented in Section 3.4 of Chapter 2 and Section 2.7 of Chapter 3, whose duration appears limited by resistive evolution of the q-profile. Figure 1.7 portrays a representative example from JT-60U in an almost steady-state, reverse-shear operation.

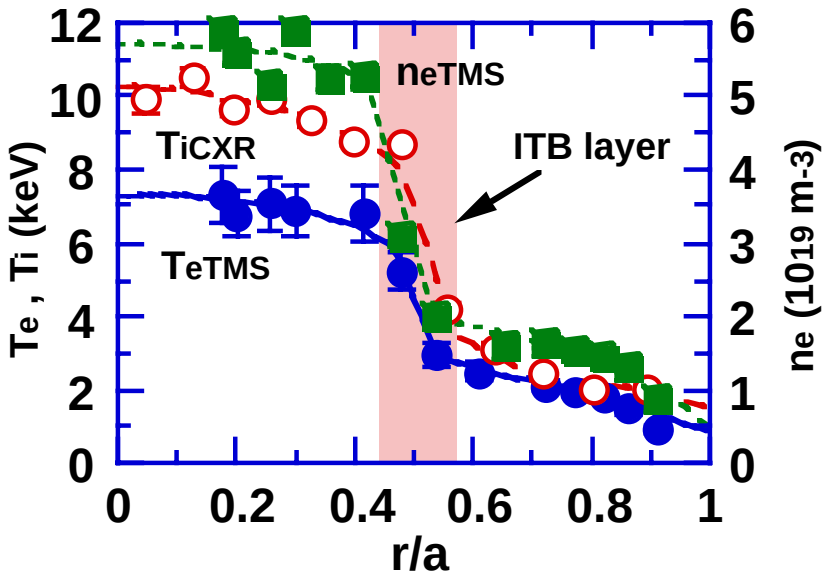

FIG. 1.7. An Internal Transport Barrier in JT-60U. For details, see Figure 8 of ref.[31].

Experiments must now focus on establishing a common internal transport barrier physics, consistent with reactor constraints (eg $T_e \approx T_i$), to provide a basis for confidence that such advanced-performance modes can be realized on a reactor-scale device. Issues concern the role of plasma shaping by elongation and triangularity, velocity-shear stabilization of microinstabilities, and the importance of deep interior, NBI fuelling. The physics of Chapters 2 and 3 both bear on the prospects for operation of ITER in a transient transport-barrier confinement mode.

Similar remarks apply to high-bootstrap-fraction, reverse-shear, steady-state modes, often called Advanced Tokamak operation. Ideal MHD stability calculations find these plasmas to be unstable to global, n=1, external kink modes for useful values of the plasma pressure ($\beta > 0.03$), unless a perfectly conducting shell closely surrounds the plasma. In principle, a finitely conducting shell will suffice, provided the plasma rotates sufficiently fast with respect to the shell so that the skin-depth is small compared to the shell thickness. Thus, data regarding plasma rotation and the associated wall stabilization of global MHD kink and resistive wall modes [33] appears to be essential to demonstrating useful plasma pressures in steady-state discharges. As explained in Section 3.3.7 below, the alternative is stabilization by active n=1 coils [34]. Section 3.3.7 of thi Chapter and Section 2.4 of Chapter 3 reports the status of this physics; a firm rotation requirement has yet to emerge.

1.3.3. Magnetohydrodynamic Phenomena, Disruptions, and Operational Limits.

In magnetically confined plasmas, magnetohydrodynamic (MHD) phenomena which have a global character play a defining role in determining the accessible parameter space and thereby setting the limits of fusion performance. Global physics processes in Region 1 govern operational limits for the core of a tokamak discharge. Chapter 3 summarizes our current knowledge of such processes, which encompass ideal MHD stability, determination of the plasma pressure limit via slow generation of magnetic island structures driven by bootstrap current as well as potential methods for their control, sawtooth relaxations of the inner core, tolerable error field limits, positional and shape control, and disruption phenomenology, including Vertical Displacement Events (VDEs) and runaway electron generation. The steep gradients in Region 2, which are characteristic of H-mode operation, cause a sequence of relaxation phenomena called Edge Localized Modes (ELMs), which are global on the scale of Region 2. Section 2.6 of Chapter 3 addresses their interpretation as MHD phenomena, while Section 3.8 of Chapter 4. evaluates the role of ELMs in power and particle control.

1.3.3.1. Magnetohydrodynamic stability

The principal global stability limits relate to the maximum plasma current, plasma density and plasma pressure, or β, which can be achieved. Attempting to exceed these limits often gives rise to major disruptions, which leads to a loss of the plasma thermal energy and a dissipation of magnetic energy on rapid timescales, typically 100μs and 10ms respectively in present experiments In addition, local stability limits give rise to MHD instabilities, such as sawteeth in the plasma centre and ELMs at the plasma edge, which can have a less severe, but nevertheless important, impact on fusion performance. In Chapter 3 it is shown that while ideal MHD theory, in which parallel electric fields are neglected, is very highly developed and sets the ultimate limits on current and β (section 3.2.1), resistive effects must generally be invoked to describe the global instabilities most commonly observed in tokamak experiments. Moreover, additional destabilizing or stabilizing effects arising from the presence of a bootstrap current, interactions with energetic particle populations, and the existence of low-level non-axisymmetric error fields can have a significant influence on MHD activity in present tokamaks and are expected to be important in reactor scale plasmas.

Although it can be shown that fundamental considerations deriving from ideal MHD theory determine the limiting parameters for the magnetic equilibrium, principally the plasma current and vertical elongation, the choice of equilibrium parameters for the ITER reference scenario, a plasma current, I_p, of 21MA, and elongation, κ, of 1.6, are based on experimental evidence and practical considerations which should apply to reactor-scale plasmas in general. It is known that a hard disruptive limit exists when the edge safety factor $q_{95} \approx 2$. However, extensive operational experience has shown that operation at $q_{95}=3$, as is foreseen in ITER, is a good compromise between the desire to maximize energy confinement by operating at high current and the increasing susceptibility to instability as q=2 is approached. This choice, furthermore, allows some margin for increasing current, if necessary, to offset degraded confinement close to operating limits.

Operation of elongated plasmas, desirable to increase confinement and ideal β-limits, requires continuous feedback control of otherwise vertically unstable plasmas. Although operation at higher elongation - $\kappa \geq 2$ - is well established in present experiments, considerations relating to power requirements for feedback stabilization of vertical displacements, constraints arising from a reactor-relevant poloidal field coil configuration, and the limitation of forces in vertical displacement events (VDEs) constrains the choice of κ.

1.3.3.2. Magnetohydrodynamic β-limits and neoclassical islands

Because fusion power production scales approximately as $\beta^2 B^4$, there is a substantial incentive to operate at the highest attainable β, a point emphasized by the requirements of steady-state operation and attractive economics in a reactor. In section 3.2.1 it is shown that the β-limit arising from ideal MHD stability, corresponding to $\beta_N=\beta/(I_p/aB)\sim3.5$ for simple, monotonic q-profiles characteristic of inductive operation, is well validated by existing experiments and allows ITER a considerable margin for operation at its design operating point of $\beta_N=2.2$. However, as discussed in detail in Section 2.3 of Chapter 3, the observation in numerous experiments in recent years of neoclassical tearing modes at β_N values well below the ideal limit poses a more significant constraint for ITER operation [35].

Since the configuration is no longer rigorously axisymmetric, these modes can change the topology of the magnetic field in the vicinity of low-order-rational magnetic surfaces to have an island structure best represented in helical flux [35]. Figure 1.8 shows the island topology in helical flux while Figure 1.9 portrays a representative waveform of neoclassical island development from a sawtooth trigger to a saturated island.

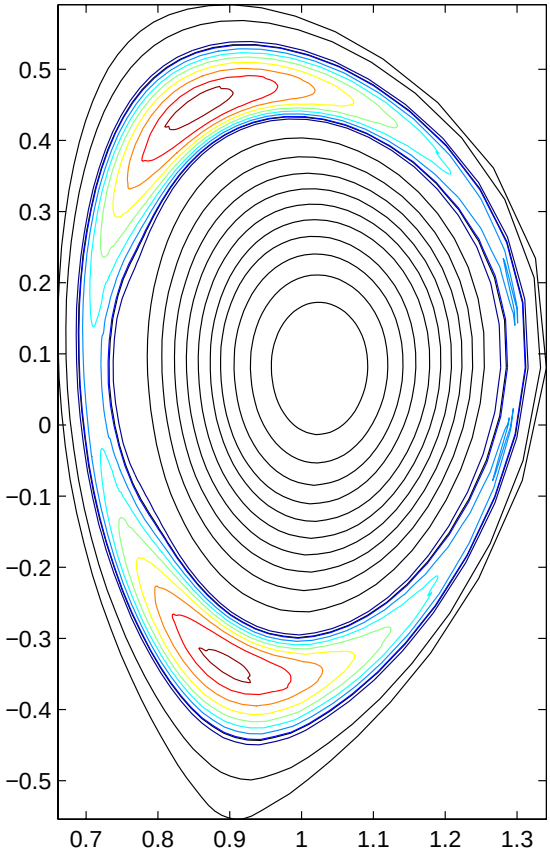

FIG. 1.8. Neoclassical Island Topology. An (m,n)=(2,1) mode is shown in helical flux [35]

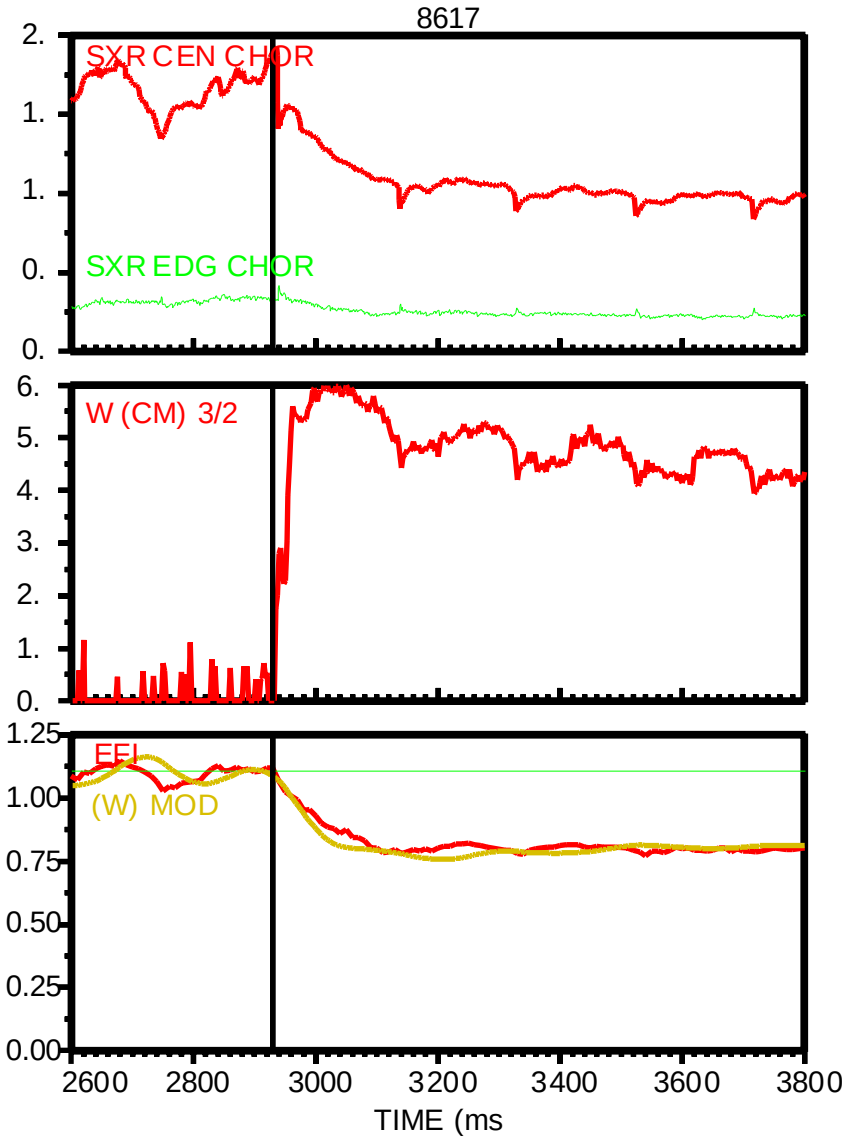

FIG. 1.9. Time waveform for neoclassical islands from DIII-D [36]. At the time of the sawtooth drop in the central soft x-ray chord (top panel), an (m,n)=(3,2) magnetic island growth is triggered (middle panel) and attains a saturated width, causing a decrease in plasma energy content (bottom panel) inferred from β_p as determined by EFIT [37] and modeled by an annular region of high thermal conductivity.

The growth of neoclassical islands arises from an instability caused by a deficit of bootstrap current inside a magnetic island due to the flattening of the pressure profile across the island, and is generally initiated by so-called 'seed' island topological changes produced by other MHD

instabilities such as sawteeth or ELMs. Fig (1.9) portrays a sawtooth crash triggering growth of an (m,n) = (3,2) island. In general, the seed island needed to initiate island growth is substantially smaller than the saturated island size, which is governed by by β_N and ν^* through their effect on the bootstrap current density. Recently, experiments have supported a polarization drift theory regarding the "onset β" value at which neoclasssical islands could grow once the relative seed island exceeds a value of order ρ^* [38]. The onset β scales as ρ^* and depends on collisionality through the combination ν^*/ρ^*.

Thus neoclassical islands occur with a range of saturated island sizes corresponding to a range of β_N-values, but their effect on plasma performance depends on β_N. In low-β_N discharges with small saturated islands characteristic of onset β-values, neoclassical islands do not affect global confinement while, in the most severe cases, generally those involving m=2, n=1 saturated islands at $\beta_N \geq 2.5$, they satisfy an island-overlap criterion which can lead to major disruptions. Although they can be observed at β_N- values in the vicinity of 2.2 in existing experiments, the present understanding of confinement degradation versus saturated island size is not adequate to allow an accurate prediction of the limiting β_N in ITER. Successful operation of long-pulse discharges in JET at the required values of $\beta_N = 2.2$ and ITER-like ν^*-values (cf Fig. 1.6) supports the ITER reference scenario. Higher $\beta_N \approx 3.0$ is experimentally accessible in the absence of sawteeth [39]. Moreover, the slow growth time of such modes in ITER, ~50s, permits in principle stabilization via electron cyclotron current drive [40,41]. Planned experiments will investigate this scheme in the near future. Initial results are encouraging [42]. Eliminating neoclassical island limitations on β could permit fusion power levels of up to 3000MW in the ITER FDR facility for periods of 50-100 s, and establish $\beta_N \approx 3.0$ as the nominal limit for inductive tokamaks.

1.3.3.3. Error field criteria

An operational limit not strictly related to the plasma state arises from the existence of small amplitude non-axisymmetric error fields, produced by residual asymmetries in the toroidal and poloidal magnet sets, which can cause a growth of resistive islands and lead to major disruptions. This phenomenon is described in section 3.2.5. The low-m (m=1,2,3), n=1 components of these error fields can instigate the growth of magnetic islands in existing experiments when the amplitude of the total error field, B_r, is ~10^{-4} of the toroidal field, B. The mechanism for the initial development of the islands is understood in terms of magnetic braking of the plasma mode rotation by interaction of the error field components with the relevant resonant q surfaces. However, at error field levels typical of moderate to large experiments only small, essentially harmless, islands should be induced and to date there is no satisfactory theoretical explanation of why such modes grow to amplitudes capable of causing disruption. An empirical scaling of the threshold field required to initiate island growth in ohmic discharges has been assembled which indicates that error fields having $B_r/B \sim 5\times10^{-6}$ - 5×10^{-5} may be critical in ITER. Current experiments also indicate that the plasma may be most susceptible to this effect during the initial low density ohmic phase and at the highest β values. Successful correction of such field errors by additional coil sets on several tokamaks underpins the proposed installation of a correction coil set capable of cancelling the m=1,2,3, n=1 error field components on ITER. This, together with the observation that external momentum injection by neutral beams improves the resilience of plasmas to such modes [43] gives confidence that error field induced modes will not limit plasma operation in ITER.

1.3.3.4. Disruptions

All tokamaks suffer from abrupt, uncontrolled events, involving rapid cooling and loss of plasma current, which have come to be known as disruptions. Accomodating the consequences of disruptions imposes significant design constraints on reactor-scale tokamaks. Section 4 of Chapter

3 details the extensive progress which has been made in understanding and quantifying the impact of disruptions on an reactor-scale device based on data from present tokamak facilities. However, modeling studies indicate that new and significant aspects of disruption physics will arise in reactor-scale devices.

Major disruptions most often occur as a terminating event when the growth of resistive MHD modes or thermal instabilities has evolved plasma parameters close to an ideal MHD limit or stochasticity threshold. On occasion, they can occur explosively — without a resistive precursor mode — when the axisymmetric equilibrium lies in close proximity to an ideal β limit. Vertical displacement events (VDEs) resulting from loss of vertical position control of the plasma constitute both a cause and a consequence of major disruptions.

It is generally accepted that disruptions occur in two stages: the thermal quench stage followed by a current quench stage [44,45]. The thermal quench stage is initiated by the growth of large amplitude magnetic islands [often (2,1) modes] within the plasma, which overlap to produce large scale ergodization of the magnetic structure, leading to a catastrophic loss of confinement. This, together with a massive influx of impurities [46], produces a rapid loss of thermal energy, expected to occur on the 1ms timescale in ITER, which causes the plasma temperature to fall to as low as 3 eV. A major fraction of the plasma thermal energy content is deposited onto the divertor chamber, causing melting and vaporization of plasma facing materials which serves as a source of impurities for the subsequent current quench stage. In the current quench stage, the plasma current decays, on a predicted timescale of ~50ms in ITER, consistent with the very substantial increase in plasma resistance. Detailed physics investigations and a large scaling database of thermal and current quench timescales assembled during of the EDA give confidence that these projections are well founded.

A new phenomenon expected to occur in reactor-scale devices is the ablation of significant material from the divertor surface in the thermal quench stage due to the large thermal energy of the plasma, ~1 GJ [47,48] Calculations show that a vapor shield should form in front of the divertor targets, dispersing the majority of the incident energy flux to the divertor chamber walls via

radiation which, in turn, causes thin melt and vaporization layers to form over the entire chamber. Divertor wall vaporization serves as an impurity source for the subsequent current quench stage.

Reactor-scale plasmas also differ from contemporary devices in the evolution of runaway electrons during the current quench phase. Analysis of energetic electron behavior in the cold, highly-impure plasmas produced by the disruption predict that a substantial runaway electron current, possibly reaching 16MA, can be generated by an avalanche process involving Coulomb scattering of thermal electrons [49]. Large skin currents might also form during this phase at the boundary between field lines in the plasma and those that contact material surfaces, giving rise to a potential further source of helical instabilities and magnetic fluctuations which could serve to inhibit runaway electron generation.

During the current quench phase, control of the plasma vertical position is generally lost and the vertical drift of the plasma induces both eddy currents in the vessel structures and so-called 'halo' currents, which flow partly in a 'halo' surrounding the plasma and partly in those elements of the vessel structure in contact with the halo plasma. The resultant electromagnetic forces on the mechanical structure can be very large, ~15000 tonnes in the most severe cases, and, in addition to a predominantly vertical force component, radial forces and toroidally asymmetric forces can occur. An extensive database of halo current observations from existing experiments has been assembled during the EDA and has guided the specification of a mechanical design capable of withstanding such substantial forces.

The trigger event for effectively all disruptions can be identified [45,50] and therefore disruptions are potentially avoidable. Various disruption mitigation schemes have been studied with the aim of dissipating the thermal and poloidal energies of the plasma in a way which avoids the most serious consequences of the disruption. Section 4.6 of Chapter 3 summarizes these schemes. Several of these have been applied in present experiments with some success. For example, the recognition that the plasma vertical stability can be maintained following a disruption if the plasma is located at the 'neutral point' of the surrounding conducting structure, has been successfully exploited in JT-60U to avoid post-disruptive VDEs [51]. Nevertheless, further R&D

is required to develop mitigation techniques capable of satisfying the very demanding requirements imposed by the disruption consequences on the reactor scale.

1.3.3.5. Sawteeth

More localized MHD instabilities will also occur in reactor-scale devices which, on the basis of experience in present experiments, are expected to have a largely benign influence. The sawtooth, which is characterized by periodic relaxations of the central electron temperature as portrayed in Fig. 1-6, falls into this class. Sawtooth activity is associated with an instability which occurs when the central q-value falls below unity and which involves a flattening of the central plasma profiles, but no global loss of plasma energy or particle content. Little impact on global plasma performance is forseen (Chapter 2, Sec. 5.1) but sawteeth may be the dominant mechanism producing seed islands needed to trigger neoclassical tearing modes, as illustrated in Fig.1-9. A detailed theoretical model of the underlying m=n=1 MHD instability, incorporating non-ideal effects such as resistivity and finite ion Larmor radius and including the stabilizing role of fast particles and thermal trapped ions, has been developed during the EDA [15] and is discussed in Section 2.2 of Chapter 3. For a reactor-scale plasma, this theory predicts that the relaxation events will occur with a repetition time of 50-100s. Although such long period sawteeth might provide the seed island for neoclassical modes, there exist various approaches to modifying sawtooth behaviour, by exploiting the heating and current drive methods available, which provide confidence that direct sawteeth effects will not limit plasma performance in ITER. The discharge of Fig. 1-6 presents an example of an ITER Demonstration Discharge whose global properties remain unaffected by sawteeth.

1.3.3.6. Edge localized modes (ELMs)

Edge localized modes are instabilities of the plasma edge (ie Region 2) associated with H-mode confinement which result in regular relaxations of the edge temperature and density profiles.

ELMs limit the maximum pressure gradient which can be reached in the narrow edge pedestal region which is a distinctive feature of the H-mode. Section 2.6 of Chap. 3 details the various forms this instability can take — called type I, type II, type III, ICRF, and grassy — and outlines the various theories which have been advanced to explain them [52] Although a theoretical description of ELM behaviour is just beginning [53, 54] and is focusing on moderate-n "peeling modes", ELMs have been well characterized empirically. The most common type of operation is with type I ELMs and the majority of the confinement database comes from this operating mode. It has the beneficial effects of regulating impurity content and density rise in a manner that has essentially allowed steady-state operation. The most significant concern is that the energy pulse produced by type I ELMs can enhance erosion of the divertor targets to the point where component lifetime becomes unacceptably short. The present database on type I ELM amplitudes, when projected to ITER, spans a range from unacceptable to acceptable in this regard. Since the ITER reference operating point has transport losses close to the H-mode power threshold, the more benign type III activity , acceptable from an erosion point-of-view, will likely prevail. Recently, it has been found that the type III regime divides into two branches: The high density branch of primary interest to ITER (DIII-D, ASDEX-Upgrade) has confinement quality that is possibly comparable to the type I regime [55]; the low density branch (DIII-D, JET) can have confinement quality strongly diminished from type I levels. It is also observed that ELMs in ICRF heated plasmas [9] are less severe than with NBI heating and acceptable for ITER operations. Alcator C-Mod, another ICRF -heated device, does not observe ELMs at all [56], but rather a region of enhanced D_α associated with the edge of H-mode plasmas. Section 3.8 of Chap 4 evaluates the implications of ELM behaviour for power and particle control.

1.3.3.7. Magnetohydrodynamics of reverse-shear and steady-state configurations

During the course of the EDA there have been rapid advances in confinement regimes which exploit modifications of the current density profile, such as reversal of the central shear, to optimze plasma performance [57-59]. Two general classes of results have been obtained. At

moderate q-values, negative central shear operation has stabilized both microinstabilies and neoclassical tearing modes. The resulting Internal Transport Barriers, as portrayed by Fig.(1-7), are quite striking and could form the basis for transient ignition in a reactor scale device. Indeed, recent experiments have reported ITBs enduring many energy confinement times [60].

Second, the leading scenarios for high-Q, steady-state operation of a tokamak reactor are low-current, high-bootstrap-fraction, reverse-shear discharges. In such discharges, the bootstrap current density profile can be well-matched to the desired plasma current density profile. Discharges of this type have been successfully maintained at low toroidal β [60, 61] . The low current of these discharges acts to increase the bootstrap fraction but increases their susceptibility to global instabilities, because their internal inductance and normalized current ($I_p/aB \approx 0.8$) are low. Many of the limitations encountered in plasma performance in such regimes are associated with global MHD modes, both ideal and resistive. The principal MHD modes observed in such regimes are discussed in Section 2.7 of Chap. 3. Infernal modes (core localized ideal kink modes), double tearing modes, and global ideal kink modes have all been identified as performance limiting instabilities in present experiments. Attainment of steady-state operation in these low-normalized-current discharges at toroidal β-values comparable to the ELMy H-mode requires high β_N values and low-n external kink modes must be stabilized by nearby conducting shells. This raises the issues of finite shell resistivity and “resistive wall modes”. In principle the low-n kinks can be suppressed by means of the sufficiently fast rotation of the plasma. However, the analysis is complicated by the existence of a slowly rotating mode whose growth depends on the proximity of a resistive shell, hence the nomenclature resistive wall mode (RWM). Recent experiments [62] find that plasmas in this wall-stabilized regime spontaneously lose their rotation in spite of continung angular momentum input by NBI and ultimately suffer an external kink mode which grows on a wall-penetration time-scale. Active n=1 feedback coils to control the spin-down and/or kink mode appear neccessary [34] . The physics of this phenomenon and its implications for steady-state operation are discussed in Section 2.4 of Chap. 3.

Further experimental investigation is required to demonstrate the necessary feedback control of the plasma current and pressure profiles necessary to avoid such instabilities and to sustain the high performance in steady-state required to meet ITER's ultimate goal of non-inductive steady-state operation.

1.3.3.8. Density limit physics

As discussed in Chapter 3.3, the ultimate limit for the plasma density is set by the growth of resistive instabilities leading to a major disruption. Non-MHD effects, principally the growth of edge and divertor radiation, which can produce radiative instabilities known as MARFEs, cause cooling of the plasma edge, contraction of the plasma current profile, and destabilization of low-m,n MHD activity which causes a major disruption in a well-established sequence of events. The role of radiation imbalance in the limiting process indicates that this limit depends on the plasma input power (including fusion power), a result demonstrated in several tokamaks. A reactor scale plasma will differ from present experiments by highly-baffled divertor configurations and large size which serve to appreciably reduce neutral particle densities inside the separatrix and raise the separatrix electron temperature, thereby potentially eliminating MARFE formation, and its effect on the current density profile.

However, of more relevance to the determination of the operating space for ignited operation in ITER is the common observation across many tokamaks that it is difficult to maintain H-mode confinement while increasing the density above the so-called Greenwald value $n_e(10^{20}m^{-3}) = I_{MA}/\pi a^2$ with gas-puff fuelling [63]. Indeed, the density limit is characterized by the lack of response of plasma density to appreciably increased gas-puff fuelling rates. Even though this limit is empirical, it is a surprisingly robust characterization of the experimental operating space. Essentially by coincidence, a reactor-scale tokamak, operating at an optimum average temperature of close to 10 keV and at its β_N-limit, has a density almost equal to the Greenwald value.

The physics mechanism of the density limit is presently not known. Pellet injection, especially high-field-side launch, can lead to Region 1 densities 20-to-50% above the Greenwald value [64] indicating that the Greenwald value is not a fundamental limit for the core. Indeed, on DIII-D, outside pellet launch coupled with divertor pumping leads to plasmas with a density 50% above the Greenwald value and confinement somewhat better than the ITER93H scaling [65]. More recent work points to the importance of pumping in the divertor private flux region. Therefore, an understanding is sought in terms of Region 2 and 3 global physics, including atomic radiation and ionization processes. Section 3.3 reviews the data and conceptual models influencing density limit physics, while Chapter 4.3.7 describes the density limit in terms of an edge operational space. A limit based on reversion from H- to L-mode is proposed, but in light of the lack of predictive theoretical models for the L→H transition, a quantitative scaling is not available.

Scaling arguments indicate that investigation of density limits in present experiments results in core plasmas with collisionalities ν^* appreciably above ITER values and potentially different confinement physics. This serves as an example of the difficulties of carrying out integrated core-edge experiments in present machines. The parameter spaces of interest to ITER for core and divertor physics are disjoint in density in present day tokamaks. These two lines evidently do meet in ITER; there, when the density reaches the Greenwald value, divertor modeling calculations show that the divertor detaches, while the core plasma collisionality remains in the low regime characteristic of ITER and the database presently being used to project confinement. Establishment of reliable operations at trans-Greenwald densities could appreciably raise ITER's fusion power output and neutron wall flux, increasing the attractiveness of the inductively-driven tokamakas as a reactor. Experiments aimed at increasing density without confinement degradation using inside pellet launch and highly baffled divertor configurations (the ITER design approach) are needed to establish a common physics of high density tokamak operations. The essential difference forseen between a reactor and present experiments such as ASDEX-Upgrade and JET is a region of finite density gradient between the H-mode pedestal and the plasma core, supported by an inside pellet

launch plasma source. The ability of inside pellet launch and shaping of the plasma periphery to support such a gradient is an area of crucial research. Reactor-scale density limits (if any) will be a key output of burning plasma physics studies. This is a rapidly devloping subject.

1.3.4. Particle Control and Power Dispersal

Power and particle control are central to the successful operation of a magnetic fusion reactor and are the subject of Chapter 4. Control of Region 1 density is the key method for regulating the fusion power output under ignited conditions. Pellet injection in turn, although it penetrates only into the periphery of Region 1, is the principal approach to core density control. High-field-side pellet launch [64] appears preferable, but is only beginning to be exploited on a regular basis. Power dispersal is required as it is well-known from the ITER/CDA studies [6] that unattenuated power outflow from a fusion reactor will lead to heat fluxes in narrow ribbons around the divertor strike points that, as a rule, cannot be accommodated by material surfaces. The ITER divertor configuration portrayed below [66] addresses both power dispersal and particle control issues.

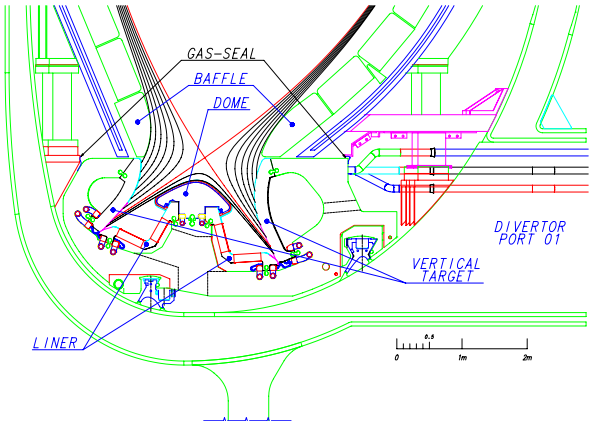

FIG. 1.10. The ITER Final Design Report Divertor Configuration. The divertor dome is in the private flux region where magnetic field lines remain in the divertor chamber. The dome acts to prevent neutral particles from entering the x-point region from the private flux region, thus reducing the prospects of x-point MARFE formation.

With respect to particle control, the configuration features a high degree of baffling with the intent of minimizing main chamber neutral gas pressures (thereby avoiding a potential source of confinement degradation) while permitting high neutral pressures in the private flux region (Region 4) which serve to increase pumping flows and exhaust helium, remove momentum from the plasma component, provide control over radiating impurity species concentrations, and effect detachment of the divertor plasma, wherein heat and particle fluxes to the divertor target plates are greatly reduced in the neighborhood of the separatrix strike points. Contemporary experiments are moving towards baffled divertor configurations, although they still lack the long leg length exposed to private flux neutral pressure which characterizes the ITER divertor, even in relative terms.

1.3.4.1. Power dispersal in divertor plasmas

Dispersal of the power outflow from a tokamak reactor in the region 3 and 4 plasma is required to reduce heat flux to a level that material surfaces designed with adequate erosion lifetime can accommodate — about 5-10 MW/m^2. Although high-heat-flux components can be designed to

withstand up to 20 MW/m^2 by making the material between the plasmas and the coolant thinner, their lifetime against erosion then becomes unsatisfactory. The strategy for power dispersal is to introduce impurity noble gas ions, such as neon, argon, or krypton (via controlled feedback loops for either pellet injection into Region 1 or gas-puff into Region 3) with the objective of attenuating the heat flux by radiation yet still providing sufficient power across the separatrix to remain in H-mode confinement. Divertor codes find that carbon impurities, sputtered physically and chemically from the graphite divertor strike plates, also radiate as part of an uncontrolled but self-regulating loop. Power dispersal by impurity radiation has been successfully implemented in contemporary tokamak experiments in which controlled impurity radiation in the mantle (the outer periphery of Region 1) and in Regions 2-4 is sufficient to partially detach the divertor plasma from the strike plates, greatly attenuating the heat flow to the strike plates [67, 68] Instead the heat flux takes the form of VUV radiation, which impinges more or less uniformly on the entire divertor chamber wall and the baffle region of the first wall near the divertor chamber. The acceptable level of mantle radiation is constrained by a requirement to maintain powerflow through the separatrix above the H-mode threshold.

Two-dimensional modeling codes applied to Regions 3-4 have shown, for a reasonable range of input parameters, excellent agreement with divertor region detachment observations and a variety of other sophisticated divertor diagnostics [69, 70]. The codes have even predicted recombination rates and electron temperature values in advance of their observation experimentally. Thus, use of two-dimensional codes constitutes the key method for projecting the performance of reactor-scale divertors in terms of “free” input parameters such as the cross field diffusivity and the “upstream” Region 3 density. These same divertor codes predict that ITER will attain the desired partially detached divertor plasmas, again for a reasonable range of input parameters [71, 72]. A theoretical scaling for the Region III-IV cross field diffusivity would serve to reduce the number of free parameters. A quantitative connection with Region 2 calls for a model of density drop across the H-mode transport barrier, which is not yet available.

Because of different scaling for core and edge physics, the core plasmas associated with detached divertor operations in present devices are usually significantly colder and more collisional than the corresponding reactor cores. In other words, the database of plasmas which exhibit detachment is largely disjoint from the database of plasmas having core nondimensional parameters β and ν^* similar to those of ITER. As Chapter 9 argues, the issue of integration of edge and core plasma physics can only be addressed experimentally in a reactor-scale device. Since direct experimental investigation of integrated core-edge physics is not presently possible, it is a special challenge to contemporary experiments and theory to provide a sufficiently detailed physics model so that the effect of divertor detachment and core density on core confinement can be reliably projected for present and reactor-scale devices.

1.3.4.2. H-mode pedestal and edge operational space

The physics of Region 2 links the SOL plasma to the main core plasma. Under nominal H-mode operations, this region contains high density and temperature gradients, which are a manifestation of the H-mode transport barrier. Observations show that the total pressure gradient is limited by a criterion to remain approximately stable against ideal MHD ballooning modes. The width of the high-gradient region determines the "pedestal" pressure just inside the transport barrier [73] This pressure, in turn, determines the energy content of the Region 2 plasma which can contribute noticeably to the total plasma energy by dint of the large volume associated with flux surfaces close to the separatrix. And, as the previous section indicates, density flow through the high-gradient H-mode transport barrier region determines the relation between (pellet) fuelling, pedestal density, and the Region III "upstream" SOL density.

A key physics issue is: What mechanism sets the width of the steep gradient region and therefore the pedestal pressure? Recent data from JET [74] indicate this depends on the hydrogen isotope , as does the type 1 ELM frequency. Because theoretical models are just beginning to be developed [75] this issue is being addressed by a database approach described in Chaps. 4.3.5-

4.3.7. More data is required before definitive extrapolations can be made, and therefore the boundary conditions for Region 1 transport calculations remain uncertain. Consequently, results of core transport simulations are usually presented with edge temperature as a parameter.

The ASDEX-Upgrade team [76] has recently introduced an Edge Operational Space Diagram portrayed in Fig.(1.11) that depicts the physics phenomenology of the pedestal part of Region 2.

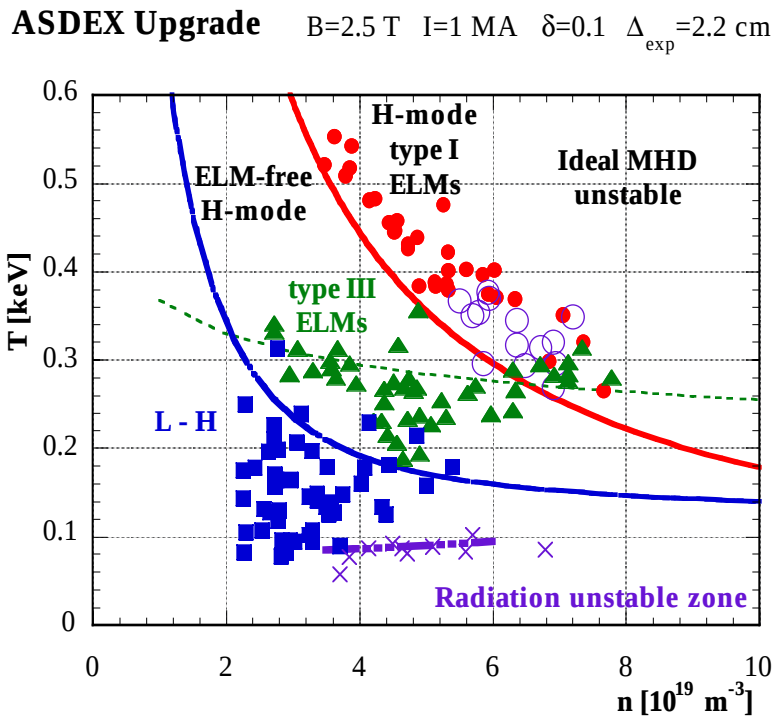

FIG. 1.11. shows the edge operational space of ASDEX-Upgrade with a triangularity (sep.) <0.1. Squares are just after the H-mode transition, triangles are Type III ELMs, circles are Type I ELMs, X are radiation unstable.

Regions are identified for various ELM types, H-mode transitions, and radiation instabilities such as MARFEs. Evidence for a constant maximum pressure pedestal for edge plasmas with Type I ELMs and a fixed magnetic configuration is quite strong. A conceptual picture for an H-mode density limit is based on the confluence of type I and type III ELM regions as density increases. However magnetic field and size scalings for these regions have not yet been

established. The next step is to construct a nondimensional edge operational space diagram which will correlate several tokamaks, with the aim of establishing the desired common physics.

1.3.4.3. Erosion of plasma facing components and tritium retention

In the present generation of tokamaks, erosion of the divertor strike plates serves as a source for impurities in the discharge, but has minimal impact on the lifetime of Plasma Facing Components (PFCs). However in reactor devices, with their much longer exposure time, erosion and redeposition will combine to limit PFC lifetimes [77]. Erosion/redeposition estimates are a major factor in the choice of PFC materials for ITER. Such estimates involve several classes of physics, including steady, partially-detached divertor operation, energy pulses arising from ELMs, vaporization and melting caused by the disruption thermal quench, and slow thermal cycles where divertor detachment is lost for ~10 s. Figure 1.12 illustrates the choice of plasma facing materials in the ITER FDR divertor design. Tungsten is the preferred plasma facing material except near the divertor strike plates because of its low sputtering rate, while CFC (Carbon Fiber Composite) is chosen for the strike-point region because it sublimes, rather than melts, during disruption thermal quenches, thereby avoiding surface irregularities which might later form hot-spots in normal steady-heat flux operation. Chapter 4.5 summarizes our knowledge of this area, which has special impact on design choices.

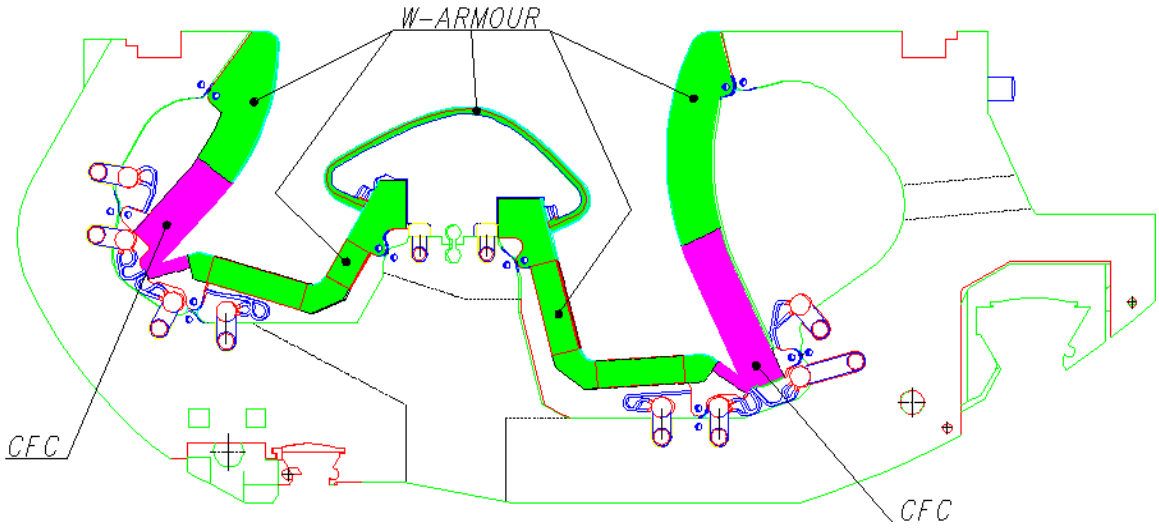

FIG. 1.12. Plasma facing materials of the FDR divertor.

The ultimate fate of tritium fuelling is of key importance to the issues of maintaining the in-vessel tritium inventory below the ≈1 kg safety limit and the sustainment of tritium self-sufficiency for a reactor. Reactor blanket neutronics designs yield a tritium breeding capability which assures tritium self-sufficiency provided 90% of the tritons injected into the core are burned, even though they may have to go through a pellet-plasma-neutral gas-pump-pellet cycle several times. Thus, if there is any retention of tritons in the wall or codeposited layers during these cycles, such as occurred in TFTR [78] and JET [11], tritium recovery and self-sufficiency become issues. Chapter 4.6.3 identifies codeposition with eroded carbon from the divertor strike points as the most likely mechanism for tritium retention and outlines potential tritium recovery techniques.

At present, our predictive capability regarding erosion and tritium retention leaves substantial uncertainties in our estimates of the erosion rates of plasma facing surfaces and of the level of codeposited tritium in reactor class experiments [79]. We therefore foresee a significant experimental program during the EDA Transition Phase on the present generation of tokamaks and during the initial proton-plasmas phase of ITER operations, when access to the machine is unhampered by activation, to better characterize and understand erosion and hydrogen retention, to

develop and test techniques to minimize hydrogen retention, and to efficiently recover hydrogen retained in the plasma facing components.

1.3.5. Energetic Particle Physics

In ITER, it is expected that the dominant heating will be via thermonuclear generation of 3.5 MeV α-particles whose energy is well above that associated with the characteristic Alfven speed $E_{Alf} = M_\alpha B^2/2\mu_o n M_{DT} \approx 1.3$ MeV. A self-heating reactor must confine these particles and Chapter 5 discusses and evaluates potential loss paths, as well as the effect of a dilute energetic particle species in destabilizing or stabilizing collective modes of the plasma. Direct particle loss by toroidal field-ripple appears controllable by design. As noted for other issues of this Chapter, present experiments are not a direct replica of ITER with respect to α-particle effects on collective modes, which range from sawteeth to Alfven eigenmodes. (The latter are discrete modes of the MHD spectrum that arise because of the periodic nature of poloidal variations of magnetic field strength, such as Toroidal Alfven Eigenmodes – TAEs). The general properties are that unstable Alfven eigenmodes in ITER will have significantly higher toroidal mode numbers and a relatively weaker drive than in present experiments. During the EDA, linear stability theory for Alfven Eigenmodes has developed to the point where remarkably accurate predictions for low toroidal mode-number-n excitations are possible [80, 81]. Extensions to higher-n find that, in ITER-class devices, Alfven eigemodes are just unstable and become quite stable with minor spreading (involving no losses) of the α-particle pressure profile [82]. Nonlinear computational programs to fully assess Alfven eigenmode physics on a reactor scale tokamak are under development. ITER-class experiments have the correct parameters to return important new physics needed by reactor designers. Experimental evidence also indicates that a related m=n=1 instability, 'fishbone' activity, which is characterized by regular coherent bursts of internal MHD modes and which is destabilized by fast particles, should not prove significant in ITER [83].

1.3.6. Auxiliary Power Physics

Reliable and effective sources of auxiliary power are an element in almost all the advances in tokamak plasma physics. Not only is the evident heating function important, but auxiliary power can also drive noninductive current, which has maintained small tokamak discharges for more than two hours [84] and is crucial to the realization of steady-state tokamak operation. Differential toroidal rotation can be driven by neutral beam angular-momentum injection and arguments are advanced that the resulting flow shear could play a significant role in determinig microinstability turbulence levels and the resulting transport [19, 85]. In present experiments, neutral injection can also provide significant fuelling of hot plasma cores and resultant high density gradients within Region 1. For ITER, appeciable NBI fuelling at 1 MeV per nucleus is prohibitive from an energy budget point-of-view. Finally, selective transfer of auxiliary power to ions has led, during the EDA, to plasmas with $T_i >> T_e$ which have greatly improved ion thermal confinement and high thermonuclear fusion rates [86]. Such regimes will be available to ITER only at low densities where the energy confinement time is comparable to the electron-ion temperature equilibration time.

Chapter 6 describes four approaches to auxiliary power in ITER.

- The advantages of fast wave auxiliary power systems [87] rest on a well-developed commercial power generation technology in the 40-100 MHz frequency range and a validated ability to calculate wave propagation and absorption by straightforward linear and quasilinear methods respectively. The PION code [88] summarizes this ability and can be used as a module in transport codes like PRETOR, which simulate the entire tokamak plasma. Fast wave current drive capabilities are restricted to central current drive where attractive efficiencies have been observed. When used in connection with ion-cyclotron absorption, fast wave methods also produce a good degree of control over heating profiles. The principal limitation of ITER fast wave system is related to the requirement of operating with a large gap (~15 cm) between antenna and plasma

separatrix, which prevents a close antenna/plasma coupling, limits the power/area that can be transmitted through a port, and enhances the sensitivity of antenna radiation resistance to variation in the Region 3 density caused by ELMs.

- Neutral beam injection [89] benefits from the spatial separation of plasma physics and beam technology. An attractive feature of the neutral beam injection is that the beam velocity distribution is known and its power level can be accurately measured. In reactor-scale tokamaks that require ~1 MeV beams to assure penetration, the beam must be created by negative-ion-beam technology. Ionization of beam particles in a tokamak plasma then leads to sources of density, energy, and angular momentum. The cross section for ionization processes are known and involve multi-step processes. Once created in the plasma, ions from neutral beams slow down and scatter in angle according to classical binary-collision physics. Confined ions execute conventional banana orbits and toroidal precessional drifts. As an energetic particle species, beam ions can undergo or excite many of the collective process identified in Chapter 5. Current drive theory is well developed. Indeed, the high level of detail with which codes can calculate beam interaction with the plasma has made NBI the power source of choice in many plasma physics experiments. By displacement of the target plasma, one can realize a good measure of control over the spatial deposition profiles. From a plasma physics viewpoint, neutral beam power is unique in two ways: as a source of angular momentum and as a source for charge-exchange processes in Region 1 from which line radiation can be exploited by diagnostics.

- Electron cyclotron auxiliary power systems [90] in the 130-200 GHz frequency range can provide reliable and predictive localized heating and current drive. Ray-tracing wave propagation codes and relativistic quasi-linear wave absorption codes are well developed and validated against experimental data. ECH methods are insensitive to Region 3 density and the proximity of the plasma to the antenna structure. The

resonance nature of the interaction, coupled with the narrow beamwidths of ECH antennas leads to very localized wave-plasma interaction regions. This provides the basis for a number of important plasma control functions such as driving off-axis current density to extend the duration of reverse-shear magnetic configurations and generating localized, modulated current density to suppress neoclassical tearing modes. At present, ECH is under-utilized in contemporary tokamaks because reliable sources are only just now becoming available. Given the slow pace of tokamak upgrades, it will take 5-10 years of experimental research before the capabilities of ECH on tokamaks are demonstrated at the power levels now enjoyed by neutral beam systems.

- In ITER-like plasmas, the principal role for lower-hybrid auxiliary power systems near a frequency of 5 GHz is off-axis current drive. A well-known accessibility criterion prevents wave propagation into the central regions, basically eliminating a heating role for lower hybrid auxiliary power. The physics governing lower-hybrid/plasma interactions on an ITER-scale device is, like ECH, straightforward ray-tracing wave propagation and quasi-linear wave-plasma interaction physics. In contrast with present experiments, single pass absorption is the norm for lower hybrid in reactor-scale plasmas. The more qualitative stochastic ray formalism is needed only for smaller plasmas of current devices, where multipass absorption prevails. A corresponding increase in confidence of ray-tracing results follows. Because both the frequency and parallel wavenumber are fixed in the proposed lower hybrid launching system [91] and because flat Region 1 density profiles are expected, the temperature profile will determine the off-axis current drive profile. Driven off-axis current is an essential element in maintaining steady-state magnetic reverse-shear profiles.

Coupling of lower hybrid power from the launcher into propagating plasma waves depends on the plasma density profile in the immediate vicinity of the launcher. This

will be known only after ITER operates. Alternative measures to create plasma close to the antenna, such as local gas puffing, must be examined for compatibility with the general strategy of maintaining low neutral densities in the main chamber. Again, these experiments must be done performed on ITER itself.

1.3.7. Physics of Plasma Diagnostics

A different set of physics processes, plasma measurement physics in contrast to plasma performance physics, governs our ability to measure plasma parameters in reactor-scale tokamak discharges. The ITER diagnostics program has established, via extensive consultation during the EDA, detailed requirements for plasma measurements, which Chapter 7 summarizes [92]. These requirements reflect the higher levels of feedback control loops and interlocks anticipated for a reactor-scale facility. By and large, the physics processes utilized for diagnostics on the present generation of tokamaks will translate to a reactor-scale device and fulfill the requirements. Indeed, most of the diagnostic techniques in routine use today will be available to ITER. There are, of course, substantial technical differences, for example radiation hardening of components, protection of mirror systems from plasma erosion and disruption debris, and the need for all in-vessel components to be maintainable with remote handling tools. Nevertheless, there remain some highly desirable, but not crucial measurements, which need new physics measurement principles to fulfill the requirements. The density of light ions, including the thermalised helium ash, is an example where, in a reactor-scale plasma, the neutral beams at a velocity appropriate to charge exchange recombination spectroscopy do not penetrate to the plasma core. Other examples include the energy and density of confined and escaping alpha particles. Possible new diagnostic physics concepts to meet some of these demands are in the research stage.

1.3.8. Physics of Plasma Control and Steady-State Operation

Chapter 8 examines, via integrated modeling calculations, the ability of proposed ITER control capabilities to implement the intended control [93] The emphasis is on adequate control throughout a complete discharge: from breakdown, which initiates plasma formation, and burn-through, wherin the plasma becomes completey ionized and fully stripped, to kinetic burn control, which attains a desirable and stable level of fusion power, and finally to non-disruptive shutdown. While this demonstration is based on the specifics of the ITER design, it is exemplary of reactor-scale operations. Its success provides confidence that there are no hidden inconsistencies in the ITER operational plans.

It is a goal for ITER to demonstrate reactor-scale steady-state if this proves possible for the tokamak. General theoretical arguments indicate that low-current, reverse-shear, high-bootstrap-fraction discharges are the best approach to steady-state operation [94]. Figure (1.13) portrays a representative equilibrium that is consistent with the ITER poloidal field coil set and vertical control capabilities [5]

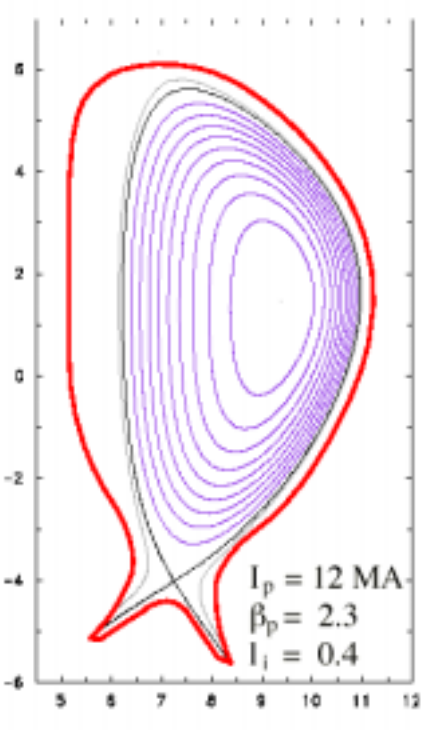

FIG. 1.13. Calculated high bootstrap fraction, reverse shear equilibrium in the ITER FDR plasma chamber.

Use of a non-chamber filling discharge permits configurations with high elongation and triangularity to investigate the physics of reactor-scale steady-state plasmas without a requirement for high Q.

Table 1.3 lists properties of this equilibrium. One notes that only modest improvements in confinement multiplier and normalized β are needed to realize this state. On the other hand, the density needed to attain the prescribed β_{tor} is considerably in excess of the Greenwald value.This is a general property of Advanced Tokamak scenarios where low current is required to reach a high bootstrap fraction.

Table 1.3. Properties of a Steady-State Discharge

Parameter	H-Mode-Like Density Profile
P_{fusion} | P_{CD} (MW)	1500 | 100
Q_{CD}	15
R_0/a (m)	8.66 | 2.32
$\kappa_{95\%}/\delta_{95\%}$	2.00 | 0.44
f_{BS}	79%
γ_{cd} ($\times 10^{20}$ A/W-m^2)	0.21
β_N | $\beta_{toroidal}$	3.8 | 3.7%
$\langle T_e \rangle_n$ | T_{eo} (keV)	12.5 | 25.9
$\langle n_e \rangle$|n_{eo} ($\times 10^{20}$ /m^3)	1.0 | 1.1
$\langle n_e \rangle / n_{\mathbf{GR}}$	1.4
τ_E (seconds)	2.46
$\tau_E/\tau_{ITER93\text{-}H}$	1.22

It should be stressed that this equilibrium is unstable in the absence of a nearby conducting shell and hence subject to the resistive wall mode [33], as discussed in Section 3.3.7. Stabilization by rotation or n=1 internal feedback coils [34] is required. Experiments on DIII-D have found that plasmas in the "wall-stabilized" regime spontaneously lose their rotation and are ultimatekly subject to an external kink mode which grows on a wall time scale [62]. For Table 1.3, the temperature, density, and current density profiles are simply assumed, in lieu of using coupled diffusion equations based on transport coefficients which are poorly known in the reverse-shear regime and can often exhibit spontaneous formation of transport barriers.

Nonetheless, Fig. (1.13) and Table 1.3 demonstrate that a reactor-scale device can have sufficient flexibility to investigate steady-state tokamak operations as its requirements are presently

understood provided provisions are made for internal n=1 feedback coils. Sections 3.2.4 and 3.3.7 discuss the resistive wall mode and the need for a more quantitative understanding of rotational or active feedback stabilization requirements. Lastly, we note again that Table 1.3 calls for a density considerably in excess of Greenwald, underscoring the importance of plasma fuelling physics to Advanced Tokamak research.

1.3.9. Summary

This Section has identified a wide range of physics processes occurring in present tokamak plasmas. It is to the credit of the fusion science effort that almost all observations can be understood, at least conceptually and often quantitatively, in terms of physics processes. The next Section will examine how thse processes will be altered and what changes in their relative importance will occur in the transition from present devices to reactor-scale facilities.

1.4. REACTOR-SCALE EXPERIMENTAL PLASMA PHYSICS

It is illuminating to regard a reactor-scale tokamak as a new scientific facility and ask: What physics issues can we anticipate investigating that are inaccessible to the current generation of tokamak facilities? Will plasma-based design requirements exceed the capability of engineering and technology to respond? The totality of issues raised by these questions comprises Reactor-Scale Plasma Physics, which can be generally defined as the physics which is dominant in reactor-scale device, with particular emphasis on those issues which cannot be investigated with contemporary tokamaks (and their evident upgrades). Of course, the proposition that there is important physics to be learned only from reactor scale devices implies that uncertainties exist in our projections for ITER plasma performance. In this way, the sources of uncertainties in plasma performance projections can be viewed as opportunities for experimental research on ITER. In the final analysis, a judicious balance must be made between projection uncertainty and research opportunity in an acceptable and useful device design.

Chapter 9 provides an extensive discussion of Burning Plasma Physics in terms of opportunities for new experimental physics which an ITER-class machine will enable. This Introduction outlines our principal arguments and illustrates them with selected examples.

It is useful to divide Reactor-Scale Plasma Physics into three elements: 1) Energetic Particle Physics, 2) Self-Heating and Thermal Stability, and 3) Scale-Dependent Plasma Physics. The last arises from the difference in physics engendered by the fact that a reactor must have a substantially larger magnetic field strength and size than present devices. Let us turn to a brief description of these three elements.

1.4.1. Energetic Particle Physics

Superficially, it would appear that the presence of energetic particles, specifically 3.5 MeV α-particles, is a key difference between present devices and a burning plasma. These particles have a centrally-peaked profile, transfer their energy to the ambient electrons, and have a characteristic velocity that exceeds the Alfven velocity of the thermal plasma. As such they are capable of interacting with discrete stable MHD modes known as Alfven Eigenmodes, destabilizing them through α-particle expansion free energy. Since current tokamaks are also heated by energetic particles which are created by fast-wave minority ion cyclotron heating or neutral beam injection, one must ask: How is it anticipated that energetic particles physics in reactor scale devices will differ from that in contemporary tokamaks, when the operational conditions are such that the characteristic velocity of the energetic particles exceeds the Alfven velocity? (Usually this means negative-ion beam injection or minority fast wave heating.) First, it is evident that the fundamental drive is weaker in reactor scale devices because the relative fast particle concentration n_f/n is given by

$$\frac{n_f}{n} = \left(\frac{2T}{E_f}\right)\frac{\tau_f}{\tau_E} \qquad (4\text{-}1)$$

where τ_f is the fast particle slowing down time and E_f its characteristic energy. Based on values presented in Table 1.1 and Table 1.2, the relative fast particle energy density in a reactor scale device is approximately a factor-of-10 less than in present devices. Some dissimilarities arise because of the isotropic velocity distribution of the α-particles differs from the anisotropic distribution arising from neutral injection or ion-cyclotron sources. Theory also permits a weaker wave particle interactions of for $v \approx 0.3 \cdot V_{Alfven}$ which can excite Alfven eigenmodes even when the auxiliary heating system fails to produce particles with $v \geq V_{Alfven}$. These differences can be accounted for by theory, which has been a remarkably good guide [80, 81] for linear stability. The key difference of energetic particle physics in burning plasma devices derives from the third element of burning plasma physics — that the scale of the device is larger than that of present devices — and not just from the presence of super-Alfvenic particles, which are found at greater relative densities in current devices. As Chapter 5 explains, the unstable toroidal mode numbers in reactors are expected to be appreciably higher because of the device size, and reactor scale devices may exhibit multi-mode Alfven Eigenmode turbulence.

The 3.5 MeV energy of α-particles does have the important consequence of transferring their energy directly to electrons, which precludes operational modes with $T_i >> T_e$ often found with neutral beam injection heating in current devices.

1.4.2. Self-Heating and Thermal Stability

Controlled, steady-state operation of a fusion plasma implies that transport power loss from Region 1 balances the sum of self-heating from α-particles and auxiliary heating power. A thermally stable solution further requires that the transport power losses increase more rapidly with temperature than the sum of the fusion power and auxiliary power, assuming a feedback loop that decreases auxiliary power (if any) as α-particle power increases. Appendix A derives a formula for the transport power losses which is equivalent to the ITER98H(y,1) confinement scaling relation Eq.(1.3.2-1) and is

$$P_{loss}(MW) = \left(1.8\cdot 10^{5}\right) \frac{n_{20}^{1.6}\, T_{10}^{2.86}\, R_m^{0.11}\, \kappa^{0.8}}{B_T^{3.03}\, M^{0.37}\, H_H^{2.86}} \left(\frac{aB}{I}\right)^{2.6} \left(\frac{a}{R}\right)^{1.49} \qquad (1.4.2\text{-}1)$$

where n is in units of $10^{20}m^{-3}$, T is the volume-average temperature in keV, P is in MW, and I in MA. The strong increase of transport losses with temperature is the factor that permits a stable thermal equilibrium in the presence of a thermonuclear reaction rate that is increasing (but less rapidly) with temperature. Since the fusion power increases as n^2 while transport losses increase as $n^{1.6}$, higher density will lead to higher fusion powers in thermal steady-state. For ignited operation with no auxiliary power, the relation is approximately $P \propto n^{3.2}$. In actual operation, the constant H_H could change abruptly, reflecting a change in confinement mode or the creation of an internal transport barrier. In this case, the density will have to respond to maintain a steady fusion power. Clearly, demonstration of thermal control will be an essential part of burning plasma physics. The characteristic time scales are the energy confinement time and the central density buildup time scale in response to peripheral plasma fuelling. The latter time scale is not well characterized by an experimental database and, in all likelihood, depends on the fueling method.

For the case of steady-state operation of a tokamak, self-heating generalizes to self-generation of plasma (bootstrap) current via pressure gradients and the degree of self-consistency between the required current density profile and the bootstrap current density profile. The current density profile, in turn, controls internal transport barriers which close the loop via their influence on pressure gradients and hence the bootstrap current. Two time scales exist in this system, the energy/density scale and the magnetic flux diffusion scale. Only with very long pulses appreciably exceeding magnetic flux diffusion times (~300 sec for ITER parameters) will definitive data regarding the prospects for steady-state operation of a reactor be available.

1.4.3. Scale-Dependent Plasma Physics

The size, plasma current, and magnetic field strength of a tokamak device in which fusion power balances transport losses can change the relative importance of physics processes and can introduce qualitatively new physics which is negligible in present devices. Chapter 9 discusses the consequences of scale in considerable detail. This Introduction gives five illustrative examples to convey the importance of size to the investigation of Reactor-Scale Plasma Physics. We note that we have already argued that plasma scale is the dominant parameter regarding the difference in energetic-particle, Alfven-eigenmode physics between present devices and a reactor.

Our first example concerns the scaling of the plasma density relative to the Greenwald value in ITER Demonstration Discharges such as portrayed by Fig. 1.6. The Greenwald-normalized density is defined by

$$\frac{n}{n_{GR}} = \frac{n_{20}\,\pi\,a^2}{I_{MA}} = \left(\frac{4\pi}{10}\right)\frac{n_{20}\,R\,q}{B\left(1+\kappa^2\right)} \qquad (1.4.3\text{-}1)$$

The combination of definition (1.4.3-1) with the constant β and ν^* scaling of (1.3-3) indicates that if a reactor is at the Greenwald density value, as ITER parameters indicate, then Demonstration Discharges in present experiments at identical β and ν^* values must have densities appreciably below the Greenwald value. Thus, the integrated system of core confinement and edge density limit physics can only be directly investigated on a reactor- scale device.

The second illustration is again an example of the coupling between core and edge physics processes and involves changes in proximity to operational boundaries. Chapter 2 presents empirical scaling relations for two powers: the transport power loss from an H-mode discharge and the power flow through the separatrix required to maintain H-mode edge conditions. The scaling of these two powers differs [95]. For ITER Demonstration Discharges in present devices, which are prepared to have core values of β and ν^* identical to those anticipated for ITER, the transport power loss considerably exceeds the requisite H-mode power threshold, thereby assuring

operation in H-mode. For an ITER-scale plasma, these two powers are roughly equal and questions arise as to whether operation near the threshold power boundary will realize the full benefits of H-mode confinement. Of course, one can always reduce auxiliary power to operate near threshold in present devices, but then the core β and ν^* values will differ from those of ITER, potentially changing core confinement.

The general conclusion is that definitive experimental investigations of interactions among diverse plasma processes in the core and edge can only be achieved in reactor-scale devices. Note that the divertor plasma of the ITER Demonstration Discharge in Fig.(1.6) is attached, not detached. Sections 1.3.4.1 and 4.3.3 remark the present database for core confinement is disjoint with detached divertor database. Thus, integrated experimental investigations of core-edge compatibility constitute an important part of Reactor-Scale Plasma Physics.

The third illustration concerns the thermal quench phase of full-power ITER disruptions, in which the thermal energy content of the plasma is rapidly deposited onto the plasma facing components in the vicinity of the divertor strike points. The magnitude and short duration of the pulse will cause vaporization and melting (or sublimation) of divertor strike-point material as well as a portion of the divertor chamber wall [47, 48] . This regime is not encountered in present tokamaks, where the thermal pulse associated with the thermal quench can be accommodated by the heat capacity of solid material. In the case of ITER, the vaporization occurring at the divertor strike points and surrounding areas will release carbon and tungsten into the subsequent current quench phase disruption, acting to cool this plasma and abet the formation of a runaway electron avalanche. In this case, reactor-scale plasma physics incorporates a phenomenology which is unattainable in present devices. Investigation of such plasmas is also part of burning plasma physics.

For our fourth example, we turn to the avalanche theory of runaway electron generation [49] presented in Chapter 3.4.4. The key result is that the number of avalanche e-foldings in runaway electron density is proportional to the plasma current and of order unity in present

experiments. However, in an ITER-class device, the number of e-foldings is large, making runaways generally negligible in present machines but of clear importance to reactors.

Lastly, we note that many tokamaks with internal transport barriers have plasmas with $T_i >> T_e$, which is known to reduce microinstability transport [96, 97]. This condition arises because, in present experiments with 40-100 keV beams, the neutral beam auxiliary heating power is transferred primarily to the ions. However, in reactor-class devices, the beam energy must exceed 1 MeV to assure adequate penetration. Consequently, both auxiliary and thermonuclear α-particle power flows principally to electrons. In any event, for reactor plasmas, the electron-ion equilibration time will be short compared to the energy confinement time, assuring $T_e \approx T_i$. Direct, central fuelling by neutral beams is also negligible in a reactor but often important in providing peaked density profiles for internal transport barrier discharges in present experiments. Experimental investigations of internal transport barriers and their power threshold scaling relevant to burning plasmas should focus on plasmas with negligible beam fuelling, with electron heating, and with $T_e \approx T_i$.

Taken collectively, these examples illustrate that reactor-scale plasma physics has fundamental differences from the plasma physics of present machines. Not all plasma regimes found on present tokamaks are accessible to reactor-class discharges. Reactor-class discharges can be affected by processes negligible in present devices. Undisciplined translation of plasma performance from present devices to reactor-scale facilities can be quite misleading. One can conclude that, in addition to achieving an understanding of individual physics processes, a reliable reactor physics basis must address issues of reactor-relevant integration of individual processes inaccessible to present experiments. Reactor-scale experimental physics has much to teach us.

1.5. PROJECTING ITER OPERATIONS

Fundamentally, the ITER Physics Basis is a set of projection methodologies with which to extrapolate from data provided by the present generation of tokamaks and guide the design of a reactor-scale device, as exemplified by the ITER parameters of Table 1.1. Extrapolation

methodologies are needed for codes and theoretical models as well. The goal is that the research facility which results should provide unique and essential information needed for the design of a subsequent fusion power station. This goal will be met if the methodologies are sufficiently accurate so that tokamak discharges can firstly be reliably produced, controlled, and diagnosed and secondly, have appreciable thermonuclear power and parameters close to those proposed for ITER.

ITER projection methodologies can be organized into three classes:

1. Those which bear on the issue of whether a single pulse can be reliably produced.
2. Classic plasma physics performance projections for reactor scale devices.
3. Multiple-pulse, plasma-wall erosion and tritium retention issues.

In a number of areas, our predictive ability does not suffice to permit machine operation at full parameters immediately. The usual course of gradually increasing experimental parameters and observing plasma physics and machine response should be the norm. The assessment of projection methodologies then should be based on their ability to guide such an experimental campaign and to benefit from the data returned by the observations.

1.5.1. Single Pulse Issues

The starting point for an assessment of projections regarding single-discharge issues is an assumption that the nominal plasma performance objectives will eventually be reached through a series of shots with gradually increasing parameters. The principal single-shot issues are plasma initiation, control, disruptions, thermal stability, and heat load on the divertors. The basic methodology is to use physics information to develop conservative design requirements which will assure that machine components will survive and function, even at extreme limits of projected plasma performance. For disruption physics, quantitative statements rest on databases derived from present devices, extrapolated to a reactor via straightforward arguments. In the case of toroidally asymmetric halo currents, new and definitive databases have been created which

adequately bound the problem. To evaluate divertor heat fluxes, results from two dimensional modeling codes, which replicate present divertor observations, are invoked. These codes find the desired partially detached divertor solutions for ITER-like plasmas.

Initially, discharges will be in proton plasmas, with limited auxiliary heating power (100 MW or less). Breakdown and burnthrough will be fundamentally the same in reactor-scale plasmas as in present tokamaks, with the additional help of electron cyclotron heating to assure breakdown and accelerate burnthrough. As has been the case with present tokamaks, an experimental period will likely be needed to understand the specifics of the poloidal field null formation and vertical field rampup associated with bringing the current up to and past the 1 MA level.

Accurate estimates of power dispersal and divertor plate heat fluxes will rest on 2D divertor modeling codes. Based on the impressive successes of divertor modeling codes in present day plasmas, initial low-to-moderate power proton plasma discharges should suffice to calibrate these codes and confirm, via density and power scans, their ability to predict detached divertor status for full-parameter shots. The key calibration issue is the scaling of the turbulent cross-field dffusivity which has been taken as an adjustable input in simulating present experiments. The results are sensitive to the adopted value [72]. Since proton plasmas will likely be in L-mode, there will be no need to reach a prescribed power through the separatrix in calibrating the divertor modeling codes. With a wide range of pellet and gas puff fuelling, impurity injection options, and pumping speeds, a reactor-scale facility will have considerable flexibility to optimize power dispersal and divertor heat flux solutions. The methodology to assure adequate power dispersal on a single-shot basis is sound.

Proton plasma discharges of increasing current and energy content will also calibrate our ability to evaluate disruption consequences at full parameters. Our database analyses and modeling indicate that disruptions of low-energy-content discharges with $q \approx 6$ and 100 MJ of thermal energy should be easily accommodated by designs such as that presented in the ITER Final Design Report. A calibration of our estimates of disruption consequences by observations of such

discharges should confirm our predictions that the FDR design can withstand full-parameter disruptions. Similar remarks apply to vertical position control, where q≈6 discharges will require smaller control voltages than full-parameter q≈3 shots.

Combining our present projection methodologies, which indicate no problems on a single-shot basis for low-current, low-energy-content plasmas, with data from discharges of increasing performance generates confidence that a reactor-class device can be operated at full-parameters with no adverse consequences on a single-shot basis.

1.5.2. Physics Performance Projections

Section 1.3 has made it clear that there are many plasma processes to extrapolate from contemporary tokamak plasmas to a reactor-scale device. Our assessment is that collectively the extrapolations give a sufficiently accurate guidance that the major parameters of a reactor-scale experiment can be chosen with confidence that ELMy H-mode plasma performance will lie close to the nominal projections and that tradeoffs made in reaching the major design parameters are indeed meaningful. Arguably, the major weakness is the fact the a reactor-scale tokamak operates close to the Greenwald density value and the H-mode power threshold. But confinement degradation near these boundaries is just the issue that Section 1.4 concludes needs a reactor-scale device for resolution.

Let us briefly discuss the major extrapolation methodologies for plasma performance.

1. The global confinement scaling relation collapses data from a quite diverse range of magnetic field strengths and sizes to a relation that has only 15% RSME. A very careful discussion of attendant uncertainties is presented.

2. Neoclassical tearing modes limit the long-pulse β-values and the observed magnetic fluctuations are in accord with theory. Because saturated islands depend only β and ν^*, which are similar in present discharges and ITER, the values of $\beta_N \geq 2.2$ found in

present discharges should be attainable in ITER as well. The neoclassical tearing mode β-limit is not "hard" and theoretical prospects for stabilization of neoclassical tearing modes are just now being tested experimentally.

3. The physics of the density limit is not clear, but values in excess of the Greenwald value are difficult to achieve with gas puffing. Nevertheless, pellet injection, particularly inside pellet launch [64], has led to discharges with core densities exceeding the Greenwald value. Reactor scale devices operate near the Greenwald density value and would benefit from even higher densities.

4. Experiments have demonstrated and codes have predicted that divertor detachment can be attained in present devices. The same codes give acceptable power dispersal for reactor-scale experiments. Further code validation in initial proton plasmas is planned.

5. Disruption databases have led to simple extrapolation principles. The ITER Final Design Report [4] attests to the fact that a reactor-scale device is consistent with engineering solutions that withstand disruption effects, apart from a gradual erosion in the divertor chamber. Replacement of divertor cassettes is a design feature.

6. Potential instabilities resulting from energetic α-particles can be stabilized by modest profile readjustments.

7. Subject to some uncertainty, transport losses from reactor scale experiments will exceed the H-mode power threshold, thereby establishing ELMy H-mode operations.

All of the extrapolations suggest that an ITER-like experiment will produce a burning plasma and will constitute a facility to carry out the research needed to support the design of an experimental power station. The ITER design has considerable flexibility to respond to research

results and to optimize ELMy H-mode and advanced operations at the reactor scale. A major revision of this conclusion is not foreseen as a result of future research in present devices.

1.5.3. Multiple Pulse and Erosion Issues

A reactor-scale plasma opens a new design issue in which consideration of the erosion of plasma facing components over many pulses is a key element in materials selection andthe design of plasma facing components for the first wall and divertor chamber [98]. Erosion can take place by several processes: physical and chemical sputtering in steady-state divertor operation, an increase of these processes under ELM heat loads, and vaporization and melting of divertor and baffle wall as a consequence of the heat pulse associated with a disruption thermal quench. Our projection methodologies are again 2D divertor codes that build in laboratory measurements of sputtering processes. Disruption thermal quench codes are also under development. On the basis of their predictions, calibrated against DIMES [99] and other tokamak measurements [100], an initial selection of plasma facing materials has been made for ITER, and is documented in the Final Design Report [3-5] and Fig.(1.12). The principal methodologies to optimize this choice of plasma-facing materials are associated with the fundamental device design, which has the flexibility to replace the entire divertor chamber, and in experimentation, especially during the proton plasma stage when the divertor chamber will be accessible, which will permit calibration of divertor erosion and disruption melt loss codes as well as assessment of the core concentration of impurities. Our present projections suffice to bound these issues.

Moreover, in order that the total in-vessel tritium inventory not exceed 1kg for safety considerations (using the ITER design as a guide), tritium should be recovered from tritium which has been implanted into plasma facing components or which resides in codeposited layers along with carbon sputtered or sublimated from the divertor strike plates [101]. Both TFTR and JET found a secular accumulation of tritium during their DT operations [11, 78]. Tritium recovery is addressed by Design, which provides for hot surfaces in the divertor chamber area, and by experimentation with recovery methods using basic laboratory studies, present tokamaks, and the

proton plasma phase of a reactor-scale tokamak [79] . Discharge cleaning techniques involving oxygen have been proposed. Because it is difficult to extrapolate a complex surface chemistry from present tokamaks to an ITER-like device with its very long pulse (which could self-clean plasma facing components) the precise nature of the tritium retention issue and its possible resolution must await reactor-scale long-pulse experiments. A flexible device design, incorporating elements such as the ITER divertor cassettes, divertor chamber access to measure hydrogen deposition patterns during proton plasmas, and an ability to carry out various plasma cleaning techniques with oxygen constitute the elements needed to resolve the tritium retention issue.

1.6. CONCLUDING REMARKS

Section 1.4 argues that there are essential physics differences between reactor-scale devices and contemporary tokamak research facilities. It follows that experiments on reactor-scale devices are required to provide data to support design of an experimental fusion power station. For the next step device, a judicious balance must be struck between minimizing project costs, uncertainties in performance projections, entering regimes of new plasma physics, and minimal extrapolations to a reactor. One must keep in mind that this balance will depend on the optimization goals and constraints. For example, the design which minimizes cost to attain a $Q \geq 10$ burning plasma experiment will differ from a design which minimizes the cost per unit net power output. A common key issue is: can we ascertain whether a proposed design will attain an approximate balance between heating by thermonuclear α-particles and transport power losses, thus enabling a burning plasma experiment? Based on the arguments presented in this Introduction and the material in the bulk of the Article, we conclude that the extrapolation principles now at hand and set forth in this Article provide a guidance for a design operating with ELMy H-mode plasmas. This guidance is as close to reliable as current facilities permit and key boundaries, such as the β-limit, are described accurately enough . With regard to core confinement degradation near the Greenwald-density and H-mode-power-threshold limits, scaling arguments presented in Section

1.4 indicate that direct examination of these issues is possible only in a reactor-scale device. We note that, in addition to core collisionality, plasma fuelling, divertor baffling, and edge shape (elongation and triangularity) for reactor-scale facilities differ appreciably from present devices. Establishing a common physics of inside pellet launch across a spectrum of tokamak facilities should serve to support planned operating densities. Turning to power dispersal and particle control issues, agreement between available 2D codes and experiment is sufficiently high so that these codes can determine the relative variation in divertor performance with respect to divertor leg length as function of parameters such as the SOL density. Nonetheless, continued research on present devices is needed to confirm and strengthen our confidence that the picture presented by the collection of methodologies is accurate, as well as to reduce the uncertainties and to explore prospects for active control measures such as stabilizing neoclassical modes and increasing density above the Greenwald value via inside pellet launch. Certain key theoretical and computational advances would be highly desirable to narrow uncertainties, for example a predictive theory for the L-to-H power threshold, a physics mechanism for the Greenwald density limit, and a predictive physics model for the effect of divertor detachment and core density on core confinement.

With regard to advanced and steady-state operational modes, there does not appear to be any crucial conflict regarding device designs based on ELMy H-mode physics and the flexibility foreseen as necessary to exploit whatever advanced modes future research uncovers. But the data in hand at this writing do not possess the commonality across tokamaks and performance duration to make advanced operations the design basis for nominal plasma performance.

Overall, physics research during the ITER/EDA project, which is summarized in this Article, has provided projection methodologies that permit meaningful performance assessments as well as studies of cost-performance tradeoffs of candidate designs for a burning plasma facility based on ELMy H-mode physics. It is understood that such a facility would return data on both inductive ELMy H-mode and advanced plasma operational scenarios that are essential to the design of a commercial fusion power station and can not be obtained by contemporary research facilities.

REFERENCES

[1] HOLDREN, J.P., Ann. Rev. Energy Environ., **16** (1991) 235.

[2] RAEDER, J., et al., in Safety and Environmental Assessment of Fusion Power (SEAFP) 1995. (European Commission, Brussels)

[3] Final Design Report, ITER EDA Documentation Series, (to be published) IAEA, Vienna. (1998).

[4] Technical Basis for the Final Design Report, ITER EDA Documentation Series, (to be published) IAEA, Vienna. (1998).

[5] ITER EDA Physics Design Description Documents, (available according to the intellectual property provisions of the ITER Agreement). (1998), IAEA: Vienna.

[6] POST, D.E., et al., *ITER Physics*. ITER Documentation Series, No. 21.(IAEA, Vienna, 1991).

[7] ITER EDA Agreement and Protocol 1, ITER EDA Documentation Series No. 1, IAEA, Vienna. (1992).

[8] JET TEAM (presented by M. KEILHACKER), Plasma Phys. Control. Fusion, **39** (1997) B1.

[9] START, D.F.H., et al., Phys. Rev. Lett., **80** (1998) 4681.

[10] STRACHAN, J.D., et al., Phys. Rev. Lett., **72** (1994) 3526.

[11] GIBSON, A., JET TEAM, Phys. Plasmas, **5** (1998) 1839.

[12] HAWRYLUK, R.J., Rev. Mod. Phys., **70** (1998) 537.

[13] WESSON, J., *Tokamaks*.(Clarendon Press, Oxford, 1997) 109.

[14] KADOMSTEV, B.B., Sov. J. Plasma Phys., **1** (1975) 295.

[15] PORCELLI, F., ROSENBLUTH, M. N., Plasma Phys. Control. Fusion., **40** (1998) 481.

[16] RYTER, F., H-MODE DATABASE WORKING GROUP, Plasma Phys. Control. Fusion, **38** (1996) 1279.

[17] FUKUDA, T., et al., Nuclear Fusion, **37** (1997) 1199.

[18] RIGHI, E., et. al., Plasma Phys. Control Fusion, **40** (1998) 857.

[19] BURRELL, K.H., Phys. Plasmas, **4** (1997) 1499.

[20] ZEILER, A., DRAKE, J. F., ROGERS, B., Phys. Plasmas, **4** (1997) 2134.

[21] SCOTT, B., et al. , in Fusion Energy 1998. (Proc. 17th Fusion Energy Conference, Yokohama, IAEA, 1999) Paper IAEA-F1-CN-69 Th1-05.

[22] IGITKHANOV, Y., JANESCHITZ, G., PACHER, G. W., et. al., Plasma Phys. Control.Fusion, **40** (1998) 845.

[23] CORDEY, J.G., in Fusion Energy 1998. (Proc. 17th Fusion Energy Conference, Yokohama, IAEA, 1999) Paper IAEA-F1-CN-69 EX7-1

[24] BOUCHER, D., in Proceedings IAEA Technical Committee Meeting on Advances in Simulations and Modeling of Thermonuclear Plasmas June 1992. (Montreal, Canada,) 142.

[25] CONNOR, J.W., et. al., in Fusion Energy 1996. (Proc 16th International Conf., Montreal, IAEA, Vienna, 1997) Vol. 2, 935.

[26] KINSEY, J.E., BATEMAN, G., Phys. Plasmas, **3** (1997) 3344.

[27] DIMITS, A.M., Phys. Rev. Lett., **77** (1996) 71.

[28] BEER, M.A., et al., Phys. Plasmas, **4** (1997) 1792.

[29] SYDORA, R.D., et al., Plasma Phys. Control. Fusion, **38** (1996) A281.

[30] VANDENPLAS, P.E., et al., J. Plasma Physics, **59** (1998) 587.

[31] SHIRAI, H., JT-60U TEAM, Phys. Plasmas, **5** (1998) 1712.

[32] RICE, B.W., et al., Plasma Phys. Control. Fusion, **38** (1996) 869.

[33] WARD, D.J., BONDESON, A., Phys. Plasmas, **2** (1995) 1570.

[34] NAVRATRIL, G.A., et al., Phys. Plasmas, **5** (1998) 1855.

[35] SAUTER, O., et al., Phys. Plasmas, **4** (1997) 1654.

[36] LA HAYE, R.J., SAUTER, O., Nuclear Fusion, **38** (1998) 987.

[37] LA HAYE, R.J., et al., Nuclear Fusion, **37** (1997) 397.

[38] GUNTER, S., et al., Nuclear Fusion, **38** (1998) 1431.

[39] HUYSMANS, G.T.A., et al., in in Proceed. 24th European Physical Society Conference on Controlled Fusion and Plasma Physics 1997. (Berchtesgaden) European Physical Society ,Vol. 21A, 1857.

[40] ZOHM, H., Phys. Plasmas, **4** (1997) 3433.

[41] PERKINS, F.W., et al., in 24th European Physical Society Conference on Controlled Fusion and Plasma Physics 1997. (Berchtesgaden) European Physical Society,Vol. 21A, 1017.

[42] ZOHM, H., et al., in Fusion Energy 1998. (Proc. 17th International Conference, Yokohama, IAEA, Vienna, 1999) Paper IAEA-F1-CN-69/.

[43] LA HAYE, R.J., et al., Nuclear Fusion, **32** (1992) 2119.

[44] SCHULLER, F.C., Plasma Phys. Controll. Fusion, **37** (1995) A135.

[45] WESSON, J. A., et al., Nuclear Fusion, **29** (1989) 641.

[46] WESSON, J.A., et al., Phys. Rev. Lett., **79** (1997) 5018.

[47] PESTCHANYI, S., et al., in 24th European Physical Society Conference on Controlled Fusion and Plasma Physics 1997. (Berchtesgaden) European Physical Society, Vol. 21A, 981.

[48] HASSANEIN, A., et al., J. Nucl. Mater., **241-243** (1997) 288.

[49] ROSENBLUTH, M.N., PUTVINSKI, S. V., Nuclear Fusion, **37** (1997) 1355.

[50] PAUTASSO, G., et al., in Proceed. 25thEuropean Physical Society Conference on Controlled Fusion and Plasma Physics 1998. (Praha, European Physical Society, 1998) **B169PR**.

[51] YOSHINO, R., et al., Nuclear Fusion, **37** (1997) 1161.

[52] ZOHM, H., Plasma Phys. Control. Fusion, **38** (1996) 105.

[53] CONNOR, J.W., Plasma Phys. Control. Fusion, **40** (1998) 191.

[54] CONNOR, J.W., Plasma Phys. Control. Fusion, **40** (1998) 531.

[55] OSBORNE, T.H., et. al., in 24th European Conference on Controlled Fusion and Plasma Physics 1997. (Berchtesgaden,) Vol. 21A, Part III, 1101.

[56] TAKASE, Y., et al., Phys. Plasmas, **4** (1997) 1647.

[57] RETTIG, C.L., et al., Phys. Plasmas, **5** (1998) 1727.

[58] VOITSEKHOVITCH, I., et al., Nuclear Fusion, **37** (1997) 1715.

[59] FUJITA, T., et al., Nuclear Fusion, **38** (1998) 207.

[60] GRUBER, O., et al., in Fusion Energy 1998. (Proc. 17th International Conference, Yokohama, IAEA, Vienna, 1999) Paper IAEA-CN-69/OV4/3.

[61] IDE, S., et. al., in Fusion Energy 1998. (Proc. 17th International Conference, Yokohama, IAEA, VIenna, 1999) Paper IAEA-CN-69/CD1/4.

[62] GAROFALO, A.M., et al., in Proceed. 25th European Physical Society Conference on Controlled Fusion and Plasma Physics 1998. (Praha, European Physical Society) **B094PR**.

[63] GREENWALD, M., et al., Nuclear Fusion, **28** (1988) 2199.

[64] LANG, P.T., et al., Phys. Rev. Lett., **79** (1997) 1487.

[65] MAINGI, R., et al., in Fusion Energy 1998. (Proc. 17th International Conference , Yokohama, IAEA, Vienna, 1999) Paper IAEA-CN-69/EXP2/10.

[66] JANESCHITZ, G., et al., Fusion Energy 1996, IAEA, Vienna, **2** (1997) 755.

[67] MERTENS, V., et al., Fusion Energy 1996, IAEA, Vienna, **1** (1997) 413.

[68] LOARTE, A., et al., Nuclear Fusion, **38** (1998) 331.

[69] SCHNEIDER, R., et al., in Fusion Energy 1998. (Proceed. 17th International Conference, Yokohama, IAEA, Vienna, 1999) Paper IAEA-CN-69/THP2/05.

[70] MAHDAVI, M.A., et al., Fusion Energy 1996, IAEA, Vienna, **1** (1997) 397.

[71] KUKUSHKIN, A., et al., Fusion Energy 1996, IAEA, Vienna, **2** (1997) 987.

[72] KUKUSHKIN, A.S., et al., in Fusion Energy 1998. (Proc. 17th International Conference, Yokohama, IAEA VIenna, 1999) Paper IAEA-CN-69/ITERP1/13.

[73] HUBBARD, A.E., et al., Phys. Plasmas, **5** (1998) 1744.

[74] JACQUINOT, J., et al., Nuclear Fusion, **39** (1999) 235.

[75] MILLER, R.L., et al., Plasma Phys. Control. Fusion, **40** (1998) 753.

[76] KAUFMANN, M., et al., Fusion Energy 1996, IAEA, Vienna, **1** (1997) 79.

[77] CHIOCCHIO, S., et al., in in 17th IEEE/NPSS Symposium on Fusion Engineering 1997. (San Diego,) Vol. 1, 331.

[78] MUELLER, D., et al., in 17th IEEE/NPSS Symposium on Fusion Engineering 1997. (San Diego,) Vol. 1, 279.

[79] FEDERICI, G., ANDERL R.A., ANDREW P., BROOKS, J.N., CAUSEY, R.A. et al:, to appear in Journal of Nuclear Materials, .

[80] NAZIKIAN, R., FU, G. Y., et al., Phys. Rev. Lett., **78** (1997) 2976.

[81] KRAMER, G.J., SAIGUSA, M., et al., Phys. Rev. Lett., **80** (1998) 2594.

[82] CHENG, C.Z., et al., Fusion Energy 1996, IAEA, Vienna, **2** (1997) 953.

[83] CANDY, J., et al., in in Proceed. 24th European Physical Society Conference on Controlled Fusion and Plasma Physics 1997. (Berchtesgaden,) Vol. 21A, 1189.

[84] ITOH, S., et al., Fusion Energy 1996, IAEA, Vienna, **3** (1997) 351.

[85] WALTZ, R.E., et al., Phys. Plasmas, **5** (1998) 1784.

[86] FUJITA, T., JT-60 TEAM, Plasma Phys. Control Fusion, **39** (1997) B75.

[87] ROGERS, J.H., et al., in Radiofrequency Power in Plasmas 1997. (Proc. Proc. 12th Topical Conf., Savannah, AIP, New York, 1997) 13.

[88] ERIKSSON, L.-G., et al., Nuclear Fusion, **33** (1993) 1037.

[89] HEMSWORTH, R., et al., in Fusion Energy 1996, IAEA, Vienna, **2** (1997) 927.

[90] ERCKMANN, V., GASPARINO, U. V., Plasma Phys. Control. Fusion, **36** (1994) 1869.

[91] REY, G., et al., in 17th IEEE/NPSS Symposium on Fusion Engineering 1997. (San Diego,) Vol. 1, 433.

[92] COSTLEY, A.E., et al., *Diagnostics for Experimental Thermonuclear Fusion Reactors*.(Plenum Press, New York, 1998) 41.

[93] WESLEY, J., et al., Fusion Technology, **32** (1997) 495.

[94] BOUCHER, D., et al., Fusion Energy 1996, IAEA, Vienna, **2** (1997) 945.

[95] PETTY, C.C., LUCE, T. C., Nuclear Fusion, **37** (1997) 1.

[96] KOTSCHENREUTHER, M., et al., Phys. Plasmas, **2** (1995) 2381.

[97] PETTY, C.C., et al., GA Report GA-A23114, "Dependence of heat and particle transport on the ratio of the ion and electron temperatures." (submitted to Physical Review Letters, 1999).

[98] PACHER, H.D., et al., J. Nucl. Mater., **241-243** (1997) 255.

[99] WHYTE, D.G., et al., J. Nucl. Mater., **241-243** (1997) 660.

[100] GUO, H.Y., et al., J. Nucl. Mater., **241-243** (1997) 385.

[101] BROOKS, J.N., et al., J. Nucl. Mater., **241-243** (1997) 294.

LIST OF TABLES

LIST OF FIGURES

FIG. 1.4. Thermonuclear power generation in TFTR and JET versus time from discharge initiation. The long duration JET power generation is for an ITER-like ELMy H-mode.

FIG. 1.5. Poloidal plane view of ITER, illustrating four principal regions where dominant physics differs.

FIG. 1.6. JET D-T ELMy H-mode ITER Demonstration Discharge. Normalised β, line average electron density (10^{19} m^{-3}), central electron temperature $T_e(0)$, $D\alpha$ and total power (MW) versus time for JET pulse 42756. See Table 1.2 for parameters. Divertor status was attached.

FIG. 1.7. An Internal Transport Barrier in JT-60U. For details, see Figure 8 of ref [27].

FIG. 1.8. Neoclassical Island Topology. An (m,n)=(2,1) mode is shown in helical flux [31].

FIG. 1.9. Time waveform for neoclassical islands from DIII-D [32]. At the time of the sawtooth drop in the central soft x-ray chord (top panel), an (m,n)=(3,2) magnetic island growth is triggered (middle panel) and attains a saturated width, causing a decrease in plasma energy content (bottom panel) inferred by β_p determined by EFIT [33] and modeled by an annular region of high thermal conductivity.

FIG.1.10. The ITER Final Design Report Divertor Configuration.

FIG. 1.11. shows the edge operational space of ASDEX-Upgrade with a Triangularity (sep.) <0.1. Squares are just after the H-mode transition, triangles are Type III ELMs, circles are Type I ELMs, X are radiation unstable.

FIG. 1.12. Plasma facing materials of the FDR divertor.

FIG. 1.13. High bootstrap fraction, reverse-shear equilibrium in the ITER FDR plasma chamber.

APPENDIX A

Although tokamaks are complex systems, the basic parameters are determined by simple criteria [1]. These criteria are the requirements for adequate energy confinement, for sufficient MHD stability and plasma control to avoid frequent disruptions, for adequate shielding to protect the superconducting coils from excessive nuclear heating and insulator damage, and for acceptable stresses in the toroidal field coils.

Let us turn first to energy confinement and develop a simple ignition criterion. The starting point is the assumption of ELMy H-mode operation and an energy confinement time scaling relation, IPB98(y,1), which places data from a wide range of tokamaks onto a common curve with just 15% rms deviations. The expression for the energy confinement time is

$$\tau_E = (0.0503\ \text{sec})\, H_H\, I_{MA}^{0.91}\, B_T^{0.15}\, n_{19}^{0.44}\, P_{MW}^{-0.65}\, R_m^{2.05}\, \kappa^{0.72}\, M^{0.13} \left(\frac{a}{R}\right)^{0.57} \tag{A-1}$$

where, the elongation is defined as $\kappa = S_o/(\pi a^2)$ with S_o being the plasma cross-sectional area. H_H denotes a confinement multiplier which is introduced to assess the sensitivity of results to variation in confinement. This expression can be recast to express transport losses as function of tokamak parameters

$$P_{loss}(\text{MW}) = \left(1.8\cdot 10^5\right) \frac{n_{20}^{1.6}\, T_{10}^{2.86}\, R_m^{0.11}\, \kappa^{0.8}}{B_T^{3.03}\, M^{0.37}\, H_H^{2.86}} \left(\frac{aB}{I}\right)^{2.6} \left(\frac{a}{R}\right)^{1.49} \tag{A-2}$$

where T_{10} denotes the volume-average temperature in units of 10 keV. Plasma heating by fusion α-particles can be represented by

$$P_{fusion} = (2.8\ \text{MW})\, (n_{DT,20})^2\, \langle\sigma v\rangle_{22}\, Ra^2\kappa \tag{A-3}$$

where $<\sigma v>_{22}$ denotes the volume-average fusion reactivity, including a negative contribution from bremsstrahlung losses, in units of $10^{-22} m^3/s$. It is understood that $<\sigma v>_{22}$ is a function of volume-average temperature. For the purposes of elementary estimates, we neglect fuel dilution by impurity atoms and helium ash, and equate $n_{DT} = n$. Ignition requires that

$$n_{20}^{0.4} \left(\frac{I}{aB}\right)^{2.6} R_m^{2.89} \left(\frac{a}{R}\right)^{0.51} \kappa^{0.2} B^{3.03} M^{0.37} H_H^{2.86} \max \left\{ \frac{<\sigma v>_{22}}{T_{10}^{2.86}} \right\} > 6.4 \cdot 10^4 \qquad \text{(A-4)}$$

The indicated maximization over temperature defines the most favorable temperature to ignite at fixed density. The optimized temperature is somewhat below 10 keV. For ITER FDR parameters of Table 1.1, the left hand side achieves a value of $14 \cdot 10^4$, thus assuring ignition with some margin for fuel dilution.

Fuel dilution and impurity bremsstralung do play a quantitative role and can be expressed by replacing $<\sigma v>_{22}$ by an effective reactivity $<\sigma v>_{e,22}$ in Eqs. (A-4) and (A-8). Figure A-1 presents graphs of the combinations entering Eqs. (A-4) and (A-8) for a representative fuel dilution and Z_{eff}. Here $<\sigma v>_{e,22}$ is defined via

$$< \sigma v >_{e,22} = \eta^2 < \sigma v >_{\alpha} - (0.12)\, Z_{eff} \sqrt{T_{10}}$$

where $<\sigma v>_{\alpha}$ denotes the thermonuclear contribution to the reactivity, $\eta = n_{DT}/n_e$, and the second term gives bremsstralung losses.

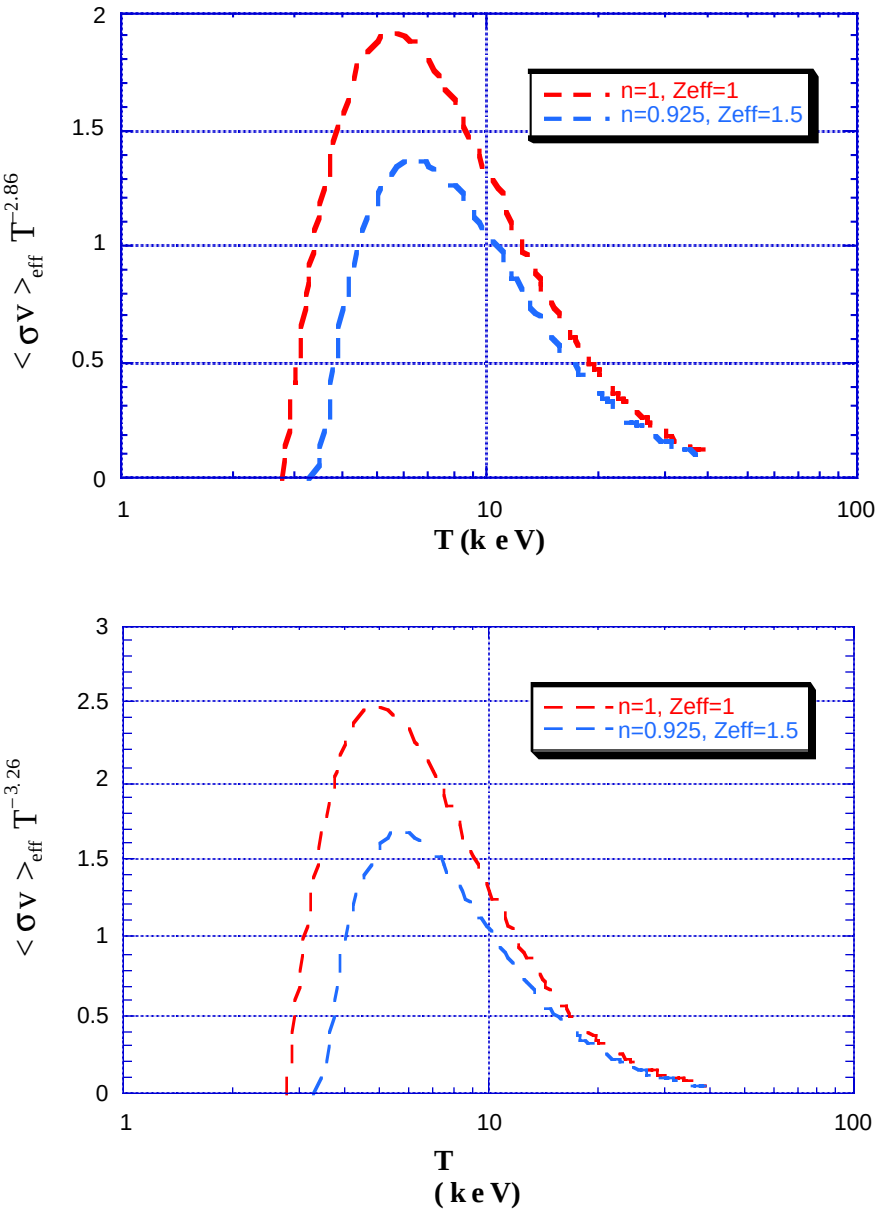

FIG. A-1. Plots of the combinations entering Eq.(A-4) and Eq.(A-8) for a pure DT plasma and for fuel dilution $n_{DT}/n_e = 0.925$ and $Z_{eff} = 1.5$.

Criterion (A-4) supposes the density to be fixed, but indicates that the higher the density, the more readily ignition is attained. There are two limits on density, the Greenwald limit and the beta limit. If one assumes the Greenwald limit, the ignition criterion can be expressed entirely in

terms of machine parameters and the nondimensional plasma performance figure-of-merit $M_{GR} = (n/n_{GR})^{0.4}\, H_H^{2.86}\, (I/aB)^{3.0}$

$$M_{GR}\, B^{3.43}\, R_m^{2.49} \left(\frac{a}{R}\right)^{0.11} \kappa^{0.2}\, M^{0.37} \max\left\{\frac{\langle\sigma v\rangle_{22}}{T_{10}^{2.86}}\right\} > 10.1\cdot 10^4 \qquad \text{(A-5)}$$

The benefits of plasma shaping and elongation are contained almost entirely in the normalized current $I_{MA}/a\, B_T$. An analysis of the H-mode confinement database has shown no explicit dependence of confinement on triangularity beyond that implicit in the normalized current. A simple version of ignition criterion (A-5) is

$$\left(I_{MA}\,\frac{R}{a}\right) > \left(\frac{46}{H_H}\right)\left\{\frac{H_H^{\,0.05}\, R^{0.21}}{B^{0.14}\, a^{0.04}\, \kappa^{0.07}\, M^{0.12}\, (n/n_{GR})^{0.13}\left[\max\left(\frac{\langle\sigma v\rangle_{22}}{T_{10}^{2.86}}\right)\right]^{0.33}}\right\} \qquad \text{(A-6)}$$

where the {} factor on the right-hand-side varies very slowly and has a value very close to unity. Thus $H_H I_{MA} R/a$ is a good figure of merit for ignition in ITER-class tokamaks. The value for the FDR design is $H_H I_{MA} R/a = 60$, which reflects fuel dilution, a finite operating space, and modest margin. For analytic estimates, the formula

$$\left(\frac{H_H\, I_{MA}\, R/a}{50}\right)^3 = \frac{Q}{Q+5} \qquad \text{(A-7)}$$

should provide a relatively transparent way to estimate fusion performance consequences. The value of $I_{MA} R/a = 50$ is ad-hoc increase over Eq.(A-6) and provides for fuel dilution, etc. When he left-hand-side of Eq.(A-7) exceeds unity, the plasma is ignited and thermal balance occurs by decreasing density below the Greenwald value or by increasing the temperature beyond the optimum value, thereby decreasing $\langle\sigma v\rangle T^{-2.86}$,.

In circumstances where the density is limited by $\beta_N = \beta_{\%}\,(aB/I)$, the ignition criterion reads

$$M_\beta\, B^{3.83}\, R^{2.89} \left(\frac{a}{R}\right)^{0.51} \kappa^{0.2}\, M^{0.37} \max\left\{\frac{\langle\sigma v\rangle_{22}}{T_{10}^{3.26}}\right\} > 28\cdot 10^4 \qquad \text{(A-8)}$$

where the plasma performance figure-of-merit is defined by $M_\beta = \beta_N^{0.4}\, H_H^{2.86}\, (I/aB)^{3.0}$. It is noteworthy that confinement performance, as measured by H_H, is more important than either the β_N -limit or Greenwald-normalized density in attaining ignition, according to (A-8) and (A-5) respectively

The purpose of this Appendix is to estimate the overall physics parameters of density, temperature, magnetic field strength, and radial build required for a tokamak to attain ignition. Radial build comprises the dimensions of the major tokamak components, central solenoid, toroidal field coils, vacuum vessel , blanket and shield, and plasma in the equatorial plane. Figure A-2 illustrates the radial build of a generic tokamak reactor.

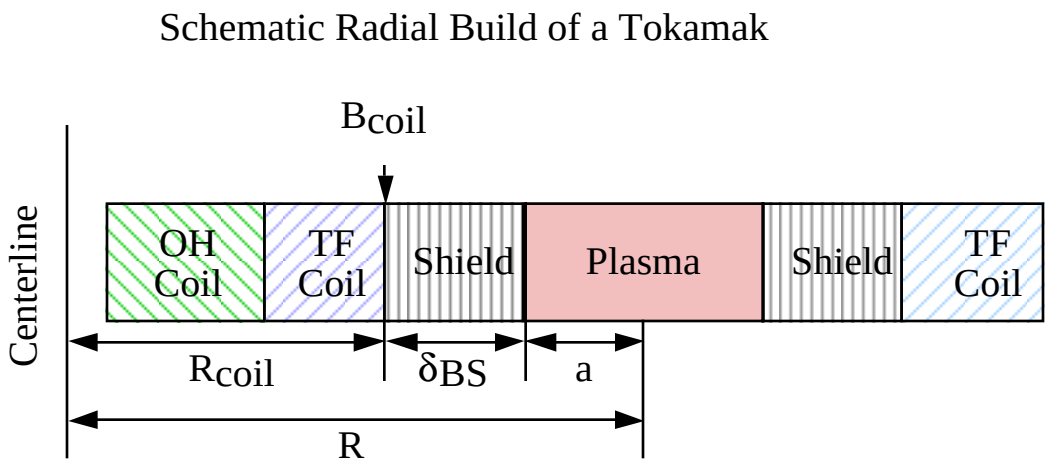

FIG. A.2. Schematic radial build of a tokamak

A combination of technological constraints arising from the maximum field permitted for superconducting magnets and the shield thickness needed to protect the magnets with the physics requirements of sufficient energy confinement and macroscopic stability determines the radial

build. It is fortunate for the prospects of magnetic fusion energy that the size needed to attain ignition is, in a broad sense, just the size needed to accommodate the required shield.

A simple equation can be derived for the size of a tokamak based on the build portrayed in Fig. A-2, the definition of the MHD safety factor q_{95}, the dependence on the plasma shape *f*, the aspect ratio, A (A=R/a, where R is the major radius and a is the minor radius), the distance δ_{BS} between the coil and the plasma inner radius including blanket and shield, and the maximum field at the inner portion of the toroidal field coil, B_c, together with the 1/R falloff of the toroidal field ($B = B_c R_c /R$) where R_c denotes the radius of the inner portion of the toroidal field coil. From Figure A-2, the plasma major radius is

$$R = R + \delta + a \tag{A-9}$$

A reasonably good fit for q_{95} for an elongated plasma is [2]

$$q_{95} = \frac{5\, a^2\, B_T}{R\, I_{MA}}\, f \tag{A-10}$$

where *f* describes the role of plasma shape through elongation κ, aspect ratio A, and triangularity δ.

$$f = \frac{1+\kappa^2(1+2\delta^2-1.2\delta^3)}{2}\,\frac{\left(1.17-0.65A^{-1}\right)}{\left(1-A^{-2}\right)^2} \tag{A-11}$$

More generally, Eq.(A-10) constitutes a definition for *f* in terms of an equilibrium solution to the Grad-Shafranov equation, with the other parameters specifying the solution.

Tokamak confinement performance is generally enhanced by lowering q_{95} and increasing the shaping function f through elongation. Both these steps serve to increase the plasma current. However, stability limits the extent to which q_{95} and κ can be varied. If $q_{95} < 2.5$, the disruptions become more frequent and confinement performance degrades relative to scaling expression (A-1). Increases in elongation lead to vertical positional instabilities that are difficult to

control if $\kappa > 1.7$ and the poloidal field control coils lie outside the toroidal field coils as Fig. 1.1 portrays. Prudent and reliable operation of a tokamak reactor suggests the values $q_{95} \approx 3$ and $f \approx 2.3$. There are also limits on the maximum magnetic field at the coil resulting from limiting fields for superconductivity as well as mechanical stress. For Nb_3Sn, we take $B_c = 12T$; for NbTi a limit of $B_c = 10T$ is appropriate. A length of $\delta_{BS} = 1.3m$ is required to shield the superconducting magnets from radiation.

Let us introduce a characteristic length a_o

$$a_o = \frac{\left(I_{MA}\frac{R}{a}\right) q_{95}}{5\, B_c\, f} \approx 1.3m \qquad \text{(A-12)}$$

where the numerical value comes from the FDR ignition condition $I_{MA}\, R/a = 60$ and the limits discussed above. Then, using Eqs.(A-9) to (A-12), one can calculate the size and aspect ratio of a tokamak that just fulfills the ignition condition via

$$\frac{R}{a} = \frac{R_c}{a_o} = A \qquad\qquad a = \left(\frac{R_c + \delta_{BS}}{R_c - a_o}\right) a_0 \qquad \text{(A-13)}$$

For an aspect ratio R/a = 3 design, the solution is

$$a = 2.6\ m \quad R_c = 3.9\ m \quad \delta_{BS} = 1.3\ m \quad R = 7.8\ m \qquad \text{(A-14)}$$

which lies close to parameters of Table 1.1.

Thus, the size and volume of ITER, or any elongated tokamak, is determined by the six parameters: plasma current, I_p and f , q_{95}, A, B_c and δ_{BS}. The first five of these enter through the combination a_o, which governs the size of the device in terms of its performance goals, expressed by $I_{MA}R/a$, and its shaping capability, expressed by f. These parameters are chosen to reflect the goals of ITER, and are influenced by physics and engineering constraints. The combination of aspect ratio and plasma current is largely determined by energy confinement requirements

according to Eq.(A-6); MHD stability and energy confinement requirements determine the edge safety factor, q; the stress limits and thermal stability margin for the toroidal field coils lead to a limit on the maximum field at the coil, B_C; the neutron shielding requirements specify the thickness of the shield and blanket, δ_{BS}. Physics choices for each of these parameters have been made by the ITER design team based on the information collected and assessed by the international fusion community through their representatives on the ITER Expert Groups as described in this Article.

REFERENCES TO APPENDIX A

[1] POST, D. E., UCKAN, N.A. Uckan, Fusion Technology **21**, 1427 (1992).

[2] UCKAN, N. A., et al., ITER Physics Design Guidelines, (IAEA, Vienna, 1990) p 10.

APPENDIX B

Article 1, ITER EDA Agreement

(1) In accordance with this Agreement, its Annexes and Protocols, the Parties, subject to their laws and regulations, shall conduct jointly the Engineering Design Activities (EDA) to produce a detailed, complete, and fully integrated engineering design of ITER and all technical data necessary for future decisions on the construction of ITER. Such design and technical data shall then be available for each of the Parties to use either as part of an international collaborative program or in its own domestic program.

(2) The overall programmtic objective of ITER, which shall guide the EDA, is to demonstrate the scientific and technological feasibility of fusion energy for peaceful purposes. ITER would accomplish this objective by demonstrating controlled ignition and extended burn of deuterium-tritium plasmas, with steady-state as an ultimate goal, by demonstrating technologies essential to a reactor in an integrated system, and by performing integrated testing of the high-heat-flux and nuclear components required to utilize fusion energy for practical purposes.

APPENDIX C

ITER Special Working Group 1

Review Report

IC-2 ROD

Attachment 5

October 1992

ITER Special Working Group 1 Review Report

Preamble

- In accordance with Article 10 of the ITER EDA Agreement,
- with reference to Sections 1 and 2 of Protocol 1,
- in the light of the Guidelines for SWG-1 imposed by the 1st ITER Council Meeting (Attachment 1),
- on the basis of the ITER Conceptual Design Activities Final Report, ITER Documentation Series No. 16, and the document referred to therein,

the Special Working Group has agreed as follows.

1 General Constraints

The ITER detailed technical objectives and technical approaches, including appropriate margins, should be compatible with the aim of maintaining the cost of the device within the limits comparable to those indicated in the final report of the ITER CDA as well as keeping its impact in the long-range fusion program.

ITER should be designed to operate safely and to demonstrate the safety and environmental potential of fusion power.

2 Performance and Testing

ITER should have a confinement capability to reach controlled ignition. The estimates of confinement capability of ITER should be based, as in the CDA procedure, on established favorable modes of operation.

- Plasma Performance

ITER should

- ♦ demonstrate controlled ignition and extended burn for a duration sufficient to achieve stationary conditions on all time scales characteristic of plasma process and plasma wall interactions, and sufficient for achieving stationary conditions for nuclear testing of blanket components. This can be fulfilled by pulses with flat top duration in the range of 1000s. For testing particular blanket designs, pulses of approximately 2000s are desirable.
- ♦ aim at demonstrating steady-state operation using non-inductive current drive in reactor-relevant plasmas.

- Engineering Performance and Testing

ITER should

- ♦ demonstrate the availability of technologies essential for a fusion reactor (such as superconducting magnets and remote maintenance);
- ♦ test components for a reactor (such as systems to exhaust power and particles from the plasma);
- ♦ test design concepts of tritium breeding blankets relevant to a reactor. The tests foreseen on modules include the demonstration of a breeding capability that would lead to tritium self-sufficiency in a reactor, the extraction of high-grade heat, and electricity generations.

3 Design Requirements

The choice of parameters of the basic device should be consistent with margins that give confidence in achieving the required plasma and engineering performance. The design should be sufficiently flexible to provide access for the introduction of advanced features and new capabilities, and to allow for optimizing plasma performance during operation. The design should be confirmed by the scientific and technological database available at the end of the EDA.

An inductive pulse flat-top capability, under ignited conditions, of approximately 1000s should be provided. In view of the ultimate goal of stead-state operation, ITER should be designed to be compatible with non-inductive current drive, and the heating system required for ignition in the first phase of operation should have current drive capability.

To carry out nuclear and high-heat flux component testing at conditions relevant to a fusion power reactor:

- the average neutron wall loading should be about 1 MW/m^2,
- the machine should be designed to be capable of at least 1 MWa/m^2 to carry out longer-time integral and materials tests.

It is desirable to operate at higher flux and fluence levels. Within the engineering margins the ITER designers should examine the implications and possibilities of exploiting a wider range of operational regimes. The design of the permanent components of the machine should not preclude achieving fluence levels up to 3 MWa/m^2. For the second phase of operation, the design should include the capability of replacing the shield with a breeding blanket.

4 Operation Requirements

The ITER operation should be divided into two phases:

- The first phase, the Basic Performance Phase, is expected to last a decade including a few thousand hours of full DT operation. This phase should address the issues of controlled ignition, extended burn, steady-state operation, and the testing of blanket modules. It is assumed that for this phase there will be an adequate supply of tritium from external sources.

  - Controlled ignition experiments in ITER will address confinement, stability and impurity control in alpha particle heated plasmas. Extended burn experiments will address, in addition, the control of fusion power production and plasma profiles, and the exhaust of helium ash.

  - The aim of current drive experiments in this phase should be the demonstration of steady-state operation in plasmas having alpha particle heating power at least comparable to the externally applied power. Using the heating systems in their current drive mode, non-

inductive current drive should be implemented for profile and burn control, for achieving modes of improved confinement, and for assessing the conditions and power requirements for the above type of steady-state operation. Depending on the outcome of these experiments, additional current drive power may have to be installed.

- Functional tests of blanket modules in this phase should consist of a few thousand hours on integral burn time, in parallel with the physics program, including continuous test campaigns of 3-6 days at a neutron wall loading of about 1 MW/m^2.

♦ The second phase, Enhanced Performance Phase, is also expected to last a decade, with emphasis placed on improving overall performance and carrying out a higher fluence component and materials testing program. This phase should address high availability operation and advanced modes of plasma operation, and may address reactor-relevant blanket segment demonstration. Operation during this phase should include continuous testing campaigns lasting 1-2 weeks, and should accumulate a fluence of at least 1 MWa/m^2.

A decision on incorporating breeding for this phase should be decided on the basis of the availability of tritium from external sources, the results of breeder blanket testing, and experience with plasma and machine performance.

The implementation of the Enhanced Performance phase should be made following a review of the results from the Basic Performance Phase and an assessment of the relative value of the proposed elements of the program.

5 Final Recommendation

The availability to achieve the above objectives and to comply with the "Guideline for SWG-1" provided by the ITER Council at its first meeting should be confirmed by the Director in the outline of the design referred to in that Guideline.

ATTACHMENT 1

GUIDELINE FOR SWG-1

The IC recommends as a general guideline for SWG-1 that detailed technical objects and technical approaches including appropriate safety margins, should be compatible with the aim of maintaining the cost of the device within the limits comparable to those indicated in the final report of the ITER CDA as well as keeping its impact in the long-range fusion program.

The IC asks the Director to present an outline of the design within about 10 months, at the time when a draft agreement of Protocol 2 should have been prepared by SWG-2.